Downloaded from http://sp.lyellcollection.org/ at University of Aberdeen on November 26, 2014

The Hudson Bay Lithospheric Experiment (HuBLE): insights into Precambrian plate tectonics and the development of mantle keels

I. D. BASTOW[1]*, D. W. EATON[2], J.-M. KENDALL[3], G. HELFFRICH[3], D. B. SNYDER[4], D. A. THOMPSON[5], J. WOOKEY[3], F. A. DARBYSHIRE[6] & A. E. PAWLAK[2]

[1]*Department of Earth Science and Engineering, Imperial College London, London SW7 2AZ, UK*

[2]*Department of Geoscience, University of Calgary, Alberta, Canada T2N 1N4*

[3]*Department of Earth Sciences, University of Bristol, Bristol BS8 1RJ, UK*

[4]*Geological Survey of Canada, Natural Resources Canada, Ottawa, Ontario, Canada K1A 0E9*

[5]*School of Earth and the Environment, University of Leeds, Leeds LS2 9JT, UK*

[6]*Centre de Recherche GEOTOP, Université du Québec á Montréal, Montréal, Québec, Canada H3C 3P8*

**Corresponding author (e-mail: i.bastow@imperial.ac.uk)*

Abstract: Hudson Bay Lithospheric Experiment (HuBLE) was designed to understand the processes that formed Laurentia and the Hudson Bay basin within it. Receiver function analysis shows that Archaean terranes display structurally simple, uniform thickness, felsic crust. Beneath the Palaeoproterozoic Trans-Hudson Orogen (THO), thicker, more complex crust is interpreted as evidence for a secular evolution in crustal formation from non-plate-tectonic in the Palaeoarchaean to fully developed plate tectonics by the Palaeoproterozoic. Corroborating this hypothesis, anisotropy studies reveal 1.8 Ga plate-scale THO-age fabrics. Seismic tomography shows that the Proterozoic mantle has lower wavespeeds than surrounding Archaean blocks; the Laurentian keel thus formed partly in post-Archaean times. A mantle transition zone study indicates 'normal' temperatures beneath the Laurentian keel, so any cold mantle down-welling associated with the regional free-air gravity anomaly is probably confined to the upper mantle. Focal mechanisms from earthquakes indicate that present-day crustal stresses are influenced by glacial rebound and pre-existing faults. Ambient-noise tomography reveals a low-velocity anomaly, coincident with a previously inferred zone of crustal stretching, eliminating eclogitization of lower crustal rocks as a basin formation mechanism. Hudson Bay is an ephemeral feature, caused principally by incomplete glacial rebound. Plate stretching is the primary mechanism responsible for the formation of the basin itself.

Gold Open Access: This article is published under the terms of the CC-BY 3.0 license.

Much of the geological record can be interpreted in the context of processes operating at the present-day plate boundaries. While the plate tectonic paradigm works well to explain processes and products during the Phanerozoic era, during Precambrian times, when the oldest rocks were forming, conditions on the younger, hotter, more ductile Earth were probably very different, making analogies with modern-day tectonics less certain. The precise onset of 'continental drift' is disputed; it has, for example, been estimated to be as early as *c.* 4.1 Ga (e.g. Hopkins *et al.* 2008), or as late as *c.* 1 Ga (e.g. Stern 2005) – a time span covering approximately two-thirds of Earth history (Fig. 1). Gathering evidence preserved deep within the plates in stable Precambrian regions (shields) is thus essential to improve our understanding of early Earth processes.

Cratonic regions are readily identified in global tomographic images where they are characterized by their deep-seated, fast wavespeed lithospheric keels. Roots can extend to depths of $\geq$250 km into the upper mantle, in contrast to the oceans and Phanerozoic continents where the plates are usually $\leq$100 km thick (Fig. 2; e.g. Ritsema *et al.* 2011). The tectosphere, or lithospheric mantle beneath a craton (e.g. Jordan 1988), is thus thought to have a thermochemical signature that differs from average lithospheric mantle, and keel formation is commonly associated with Archaean processes, such as the extraction of komatiitic magmas (e.g. Griffin *et al.* 2003), to explain the intrinsic low density of the tectosphere. It is estimated that the chemical lithosphere must be more viscous than normal mantle by a factor of *c.* 20 (Sleep 2003), enabling it to survive thermal and mechanical erosion

From: Roberts, N. M. W., van Kranendonk, M., Parman, S., Shirey, S. & Clift, P. D. (eds) *Continent Formation Through Time*. Geological Society, London, Special Publications, **389**, http://dx.doi.org/10.1144/SP389.7
© 2013 The Authors. Publishing disclaimer: www.geolsoc.org.uk/pub_ethics

Downloaded from http://sp.lyellcollection.org/ at University of Aberdeen on November 26, 2014

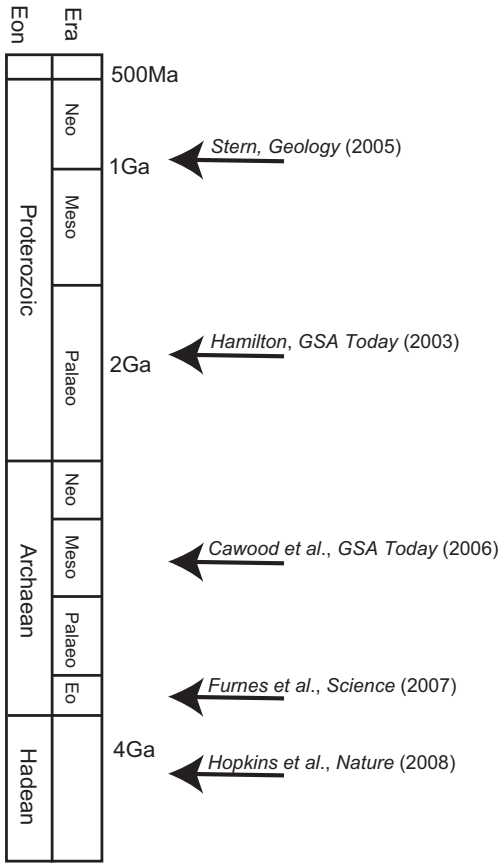

Fig. 1. Estimates of the onset of modern-style plate tectonics.

during multiple Wilson cycles over billions of years. Precisely how keels formed remains poorly understood, however.

The geological record of northern Canada spans more than 2 billion years of early Earth history (*c.* 3.9–1.7 Ga; Hoffman 1988), making it an ideal study locale for the analysis of Precambrian Earth processes. In the heart of the Canadian Shield lies Hudson Bay, a vast inland sea, which masks a significant portion of the Trans-Hudson Orogen (THO), a Palaeoproterozoic collision between the Archaean Superior and Western Churchill cratons. The THO signalled the final stages of assembly of Laurentia at *c.* 1.8 Ga (Fig. 3: Hoffman 1988; St-Onge *et al.* 2006; Eaton & Darbyshire 2010). The region is underlain by one of the largest continental keels on Earth (Fig. 2) and is also the site of one of the largest negative geoid anomalies (e.g. Hoffman 1990). The cratonic keel beneath the Hudson Bay region extends beneath both Archaean and Proterozoic terranes. How these various lithospheric subdivisions of the Canadian shield were assembled in Precambrian times, how the deep cratonic keel formed beneath them, and how the Hudson Bay basin subsequently developed within the shield, have each been difficult questions to address until recently. Hypotheses have been based principally on evidence from the geological record and potential field maps (e.g. gravity and magnetics), and seismological studies of the deeper mantle were limited by the availability of data from only two or three permanent seismic stations.

To address outstanding research questions exemplified by the Hudson Bay region, a broadband seismograph network in the Hudson Bay region was deployed by the Hudson Bay Lithospheric Experiment (HuBLE); stations have operated since 2003. The purpose of this contribution is to review the results of HuBLE, and to synthesize their implications for Precambrian processes, the formation of the Laurentian keel, and the reasons for the Phanerozoic development of the Hudson Bay basin. In addition to reviewing already-published HuBLE constraints (e.g. Thompson *et al.* 2010; 2011; Bastow *et al.* 2011*a*, *b*; Pawlak *et al.* 2011, 2012; Steffen *et al.* 2012; Snyder *et al.* 2013; Darbyshire *et al.* 2013), this contribution presents the results of a new *P*-wave relative arrival-time tomographic study of mantle wavespeed structure beneath the region.

Tectonic setting

The Canadian Shield lies in the heart of Precambrian North America. Comprising several Archaean terranes brought together during a series of orogens during the Palaeoproterozoic, the region is one of the largest exposures of Precambrian rocks on Earth (Hoffman 1988). The major phase of mountain building in the region was believed to have occurred at *c.* 1.8 Ga during the THO (Hoffman 1988; St-Onge *et al.* 2006). The Superior craton formed the indenting lower plate to the collision; the Churchill plate, presently lying to the north of the Superior craton, was the upper plate. Extensive geological mapping in recent years has added considerable detail to this two-plate picture (Fig. 3).

It is now thought that northern Hudson Bay comprises seven distinct crustal blocks, including the Superior, Rae, Hearne, Chesterfield, Meta Incognita, Sugluk and Hall Peninsula (Fig. 3; see e.g. Snyder *et al.* 2013; Berman *et al.* 2013, for a more detailed review). The Superior craton to the south is a collage of Meso- to Neoarchaean microcontinents and oceanic terranes amalgamated 2.72–2.66 Ga. The Ungava Peninsula bounds eastern Hudson Bay and exposes 3.22–2.65 Ga felsic orthogneiss and plutonic rocks that underlie *c.* 2.0–1.87 Ga volcanic and sedimentary rocks of

Downloaded from http://sp.lyellcollection.org/ at University of Aberdeen on November 26, 2014

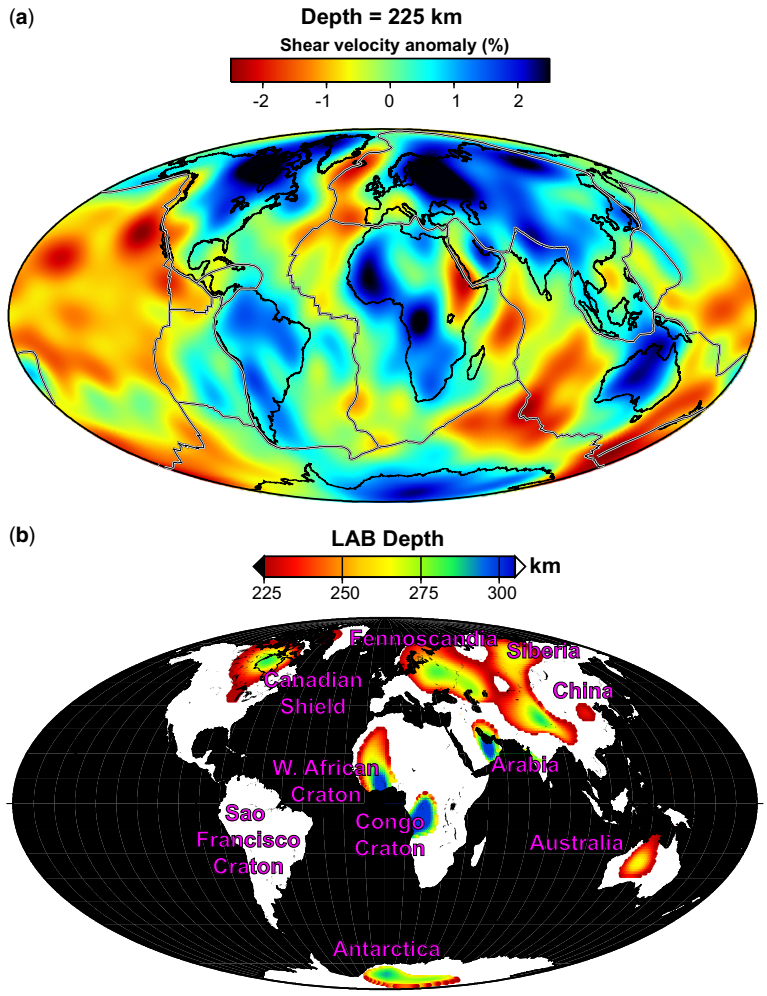

Fig. 2. (**a**) A slice at 225 km depth through the global shear wave tomographic model of Ritsema *et al.* (2011). The regions of fast wavespeed delineate the cratons world-wide. (**b**) A global view of the lithosphere–asthenosphere boundary (LAB) based on the model of Ritsema *et al.* (2011). The depth of the LAB can be defined in several ways (e.g. Eaton *et al.* 2009), but is defined here as the depth to the 1.75% fast contour. Areas of apparently thick lithosphere that are an artefact of high-wavespeed subducting slabs in the mantle are not plotted and thus appear as black (in oceanic regions) or white (in continental regions).

the Cape Smith fold belt (e.g. St-Onge *et al.* 2009, and references therein).

The Rae craton comprises Meso- to Neoarchaean, amphibolite- to granulite-facies, tonalitic to granitic orthogneisses and NE-striking *c.* 2.9–2.7 Ga greenstone belts (e.g. Jackson 1966; Wodicka *et al.* 2011*a*). The Rae is intruded by 2.72–2.68 Ga tonalite, with voluminous *c.* 2.62–2.58 Ga monzogranitic plutons (e.g. Bethune *et al.* 2011, and references therein) extending from northwestern Saskatchewan at least as far east as Melville Peninsula (Wodicka *et al.* 2011*a*). Zircon inheritance and Nd model ages of up to 3.6 Ga confirm the ancient nature of the northern Rae domain (e.g. Whalen *et al.* 2011).

The Hearne craton is characterized by *c.* 2.7 Ga mafic to intermediate volcanic rocks (e.g. central Hearne supracrustal belt; Davis *et al.* 2004) cut by *c.* 2.66 Ga granitic plutons associated with regional metamorphism (Davis *et al.* 2004). The Hearne is distinguished from Rae by its relatively young (Mesoarchaean) volcanic rocks, and by its lack of Archaean magmatism or tectonism post 2.66 Ga. The Chesterfield block (C.B. in Fig. 3; Davis *et al.* 2006) comprises *c.* 2.7 Ga supracrustal rocks and tonalite plutons, but lacks both the komatiitic

Downloaded from http://sp.lyellcollection.org/ at University of Aberdeen on November 26, 2014

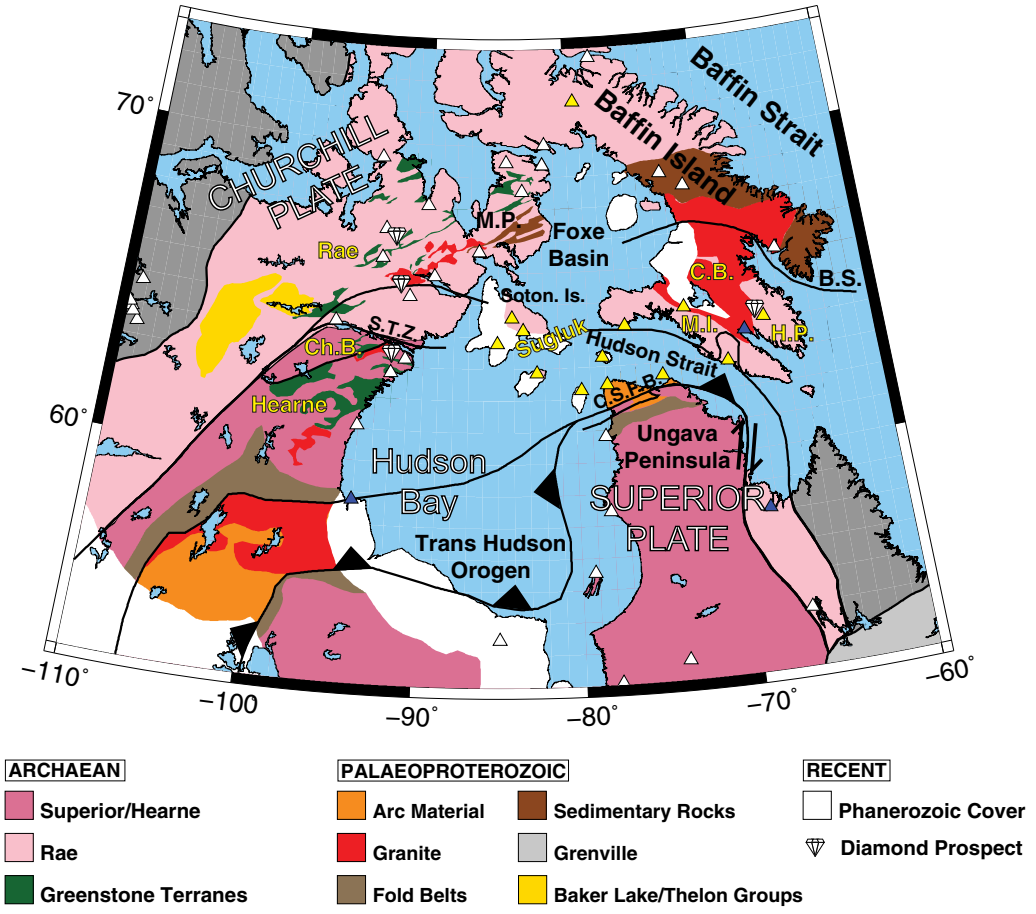

Fig. 3. Seismograph networks in northern Hudson Bay superimposed on regional geology. Ch.B., Chesterfield Block; C.B., Cumberland Batholith; B.S., Baffin Suture; C.S.F.B., Cape Smith Fold Belt; H.P., Hall Peninsula; M.I., Meta Incognita; STZ, Snowbird Tectonic Zone. Yellow triangles are HuBLE-UK stations. White triangles are POLARIS network stations. Blue triangles are permanent stations.

assemblages and evolved isotopic character of the Rae craton. The Chesterfield block is intruded by 2.6 Ga granitic plutons (Davis *et al.* 2006) that are thought to have formed after its *c.* 2.64 Ga accretion to the Rae craton (Berman *et al.* 2007). Smaller and less well understood domains in NE Hudson Bay include the Meta Incognita, Sugluk and Hall Peninsula blocks (Fig. 3).

The Meta Incognita microcontinent (Fig. 3) includes Palaeoproterozoic (2.40, 2.34–2.31, 2.15, 1.95 Ga) and lesser Neoarchaean (2.68–2.6 Ga) components (St-Onge *et al.* 2006; Wodicka *et al.* 2011*b*), overlain by Palaeoproterozoic clastic carbonates of the *c.* 1.9 Ga Lake Harbour Group (Scott 1997; Wodicka *et al.* 2011*b*). The Sugluk block (e.g. Corrigan *et al.* 2009, and references therein) includes Mesoarchaean crust that crops out on SW Baffin Island and nearby islands in Hudson Bay. It is inferred from evolved Nd signatures to underlie the northern tip of Quebec (e.g. Corrigan *et al.* 2009) where it is heavily intruded by younger *c.* 1.86–1.82 Ga plutons (St-Onge *et al.* 2006). Corrigan *et al.* (2009) suggested that it may extend west under Hudson Bay to merge with a gravity high referred to as the 'Hudson protocontinent' (Roksandic *et al.* 1987; Berman *et al.* 2005). Hall Peninsula, southeastern Baffin Island, exposes Mesoarchaean crust (2.92–2.8 Ga zircon crystallization ages; Scott 1997) which, given its spatial distribution, is tentatively considered a separate crustal block (e.g. Whalen *et al.* 2010). Amalgamation of Meta Incognita and the Sugluk block is postulated to have occurred in an intra-oceanic setting shortly before *c.* 1.9 Ga (Wodicka *et al.* 2011*b*). The Hall Peninsula block was also considered to be a part of this composite block, which is referred to by

Downloaded from http://sp.lyellcollection.org/ at University of Aberdeen on November 26, 2014

Snyder *et al.* (2013) as the Meta Incognita–Sugluk–Hall Peninsula (MISH) block. This composite block, as well as the adjacent Rae, is intruded by voluminous charnockitic rocks of the 1.865–1.845 Ga Cumberland Batholith, thought to have formed by deep crustal melting subsequent to lithospheric delamination (Whalen *et al.* 2010). Younger, *c.* 1.83 Ga plutons form late syn- to post-tectonic plutons across southern Baffin and Southampton Islands (e.g. St-Onge *et al.* 2006).

The crustal blocks surrounding Hudson Bay region have been affected by four major tectonic/metamorphic events between 2.56 and 1.8 Ga (see Berman *et al.* 2010*a*, for a detailed summary and metamorphic maps). The oldest event, the 2.56–2.50 Ga MacQuoid orogeny, affected the Chesterfield block and adjacent southeastern flank of the Rae craton. The 2.5–2.3 Ga Arrowsmith orogeny (Berman *et al.* 2005, 2010*a*; Schultz *et al.* 2007) affected much of the western side of the Rae craton from northern Saskatchewan through Boothia Peninsula to northern Baffin Island (Berman *et al.* 2010*a*, 2013). The 2.0–1.9 Ga Thelon orogeny (Hoffman 1988) affected the westernmost Rae craton, including northern Boothia Peninsula (Berman *et al.* 2010*a*). The most widespread tectonic/metamorphic reworking of the Hudson Bay region occurred during the 1.9–1.8 Ga Hudsonian orogeny (e.g. Hoffman 1988; Berman *et al.* 2010*b*) when accretion of microcontinents to the SE flank of the Rae craton occurred *c.* 1.9–1.87 Ga. These tectonic events are known collectively as the Snowbird phase of the Hudsonian orogeny (Berman *et al.* 2007).

Proposed under-thrusting of the Superior craton beneath the Churchill collage and the Cape Smith belt was initiated by *c.* 1.82 Ga (St-Onge *et al.* 2006). Palaeozoic events include deposition of carbonate rocks, presently estimated to be up to 1.5 km thick, on crystalline basement rocks of Hudson Bay, western Southampton Island, and nearby Coats and Mansel islands. At least five separate, potentially diamondiferous, kimberlite fields are known to have erupted during the Mesozoic and Cenozoic, providing mantle xenoliths and garnet xenocrysts that sample the mantle below the study area (Fig. 3).

Previous seismological studies of the Canadian Shield

The first constraints on the seismic structure of the Hudson Bay region were presented in the early 1960s by Brune & Dorman (1963) using surface-wave dispersion computed from two-station paths typically thousands of kilometres long. Hobson (1967) and Ruffman & Keen (1967) subsequently studied crustal structure using controlled source data recorded by both land and sonobuoy recorders. Since then, several studies have mapped wave-speeds beneath the Canadian Shield using surface waves in regional to global-scale models. In general the global models use data from permanent seismograph networks, resulting in reduced resolution beneath the Bay region; the two or three seismograph stations contributing to the inversions yield a limited number of surface wave paths across the shield (e.g. Megnin & Romanowicz 2000; Shapiro & Ritzwoller 2002; Lebedev & van der Hilst 2008). They indicate that Hudson Bay is underlain by a *c.* 200–300 km deep fast wavespeed mantle keel (e.g. Lebedev & van der Hilst 2008; Li *et al.* 2008; Nettles & Dziewonski 2008; Ritsema *et al.* 2011). Continent-scale models such as those of Bedle & van der Lee (2009) and Yuan *et al.* (2011) also indicate a deep-seated, fast wavespeed mantle keel beneath the Canadian Shield.

Some of the tomographic inversions take seismic anisotropy into account, but the results are variable. The model of Debayle *et al.* (2005), for example, yields east–west fast anisotropic directions beneath the Bay region, while the model of Marone & Romanowicz (2007) indicates NW–SE fast directions in the same depth interval, rotating to NE–SW at 300 km. Yuan *et al.* (2011) presented a continent-scale model of seismic heterogeneity within the North American craton, using joint inversions of long-period waveforms and SKS splitting data. They found evidence for a two-layered lithosphere. The 150–200 km-thick upper layer has fast polarization directions correlated with trends in surface geology, and was interpreted as the chemically depleted 'lid' of the shield. The lower lithospheric layer, with different anisotropic characteristics, was interpreted by Yuan *et al.* (2011) as a significantly younger, less-depleted thermal boundary layer. The Yuan *et al.* (2011) model attributes anisotropic fast polarization directions at asthenospheric depths to anisotropic fabric development owing to absolute plate motion. This model places the lithosphere–asthenosphere boundary (LAB) at a depth of *c.* 200 km depth everywhere beneath the Bay region and throughout the entire Canadian Shield, based on the anisotropic stratification of the upper mantle model.

S to *P* receiver function studies (Rychert & Shearer 2009; Abt *et al.* 2010; Miller & Eaton 2010; Kumar *et al.* 2012) provide support for an abrupt change in seismic wavespeed at *c.* 80–150 km depth across much of North America. If interpreted in the context of the two-layered lithosphere hypothesis of Yuan *et al.* (2011) or Darbyshire *et al.* (2013), this feature probably represents a mid-lithospheric discontinuity beneath cratonic North America.

Downloaded from http://sp.lyellcollection.org/ at University of Aberdeen on November 26, 2014

The *c.* 200–260 km lithospheric thickness in central and northern Canada inferred in the surface wave studies is corroborated by estimates of the thermal boundary layer, as inferred from joint interpretation of surface heat flow and *S*-wave travel time delays (e.g. Lévy *et al.* 2010). Although based on sparse data coverage, heat flow data from northernmost Ontario and central-northern Quebec are the lowest anywhere across the Canadian Shield. The thickness of the thermal lithosphere beneath the Canadian Shield varies regionally by up to *c.* 100 km (Artemieva 2006; Lćvy *et al.* 2010).

Previous studies of the mantle transition zone beneath the Canadian Shield were limited to imaging the receiver-side structure using a small number of permanent stations located large distances apart (Bostock 1996; Chevrot *et al.* 1999), geographically restricted temporary networks (Li *et al.* 1998) or global studies utilizing mid-point reflections from distant source–receiver combinations (e.g. Gossler & Kind 1996; Gu *et al.* 1998; Flanagan & Shearer 1998; Gu & Dziewonski 2002; Lawrence & Shearer 2006). Several of these studies showed that the transition zone structure was uniform across the region (less than ± 5 km; Bostock 1996), yet sparse geographical coverage of receiver functions or lower resolution (*PP* and *SS* precursors) meant that it was unclear whether this pattern was true beneath large swathes of the shield.

On a more local scale, the Teleseismic Western-Superior Transect (TWIST; see Kendall *et al.* 2002 for a review) experiment deployed 11 short-period and 14 broadband seismometers along a 600 km line in the Superior region of SW Hudson Bay in May–November 1997. A further three broadband stations were deployed further north on the Hudson Bay coastline (e.g. Kay *et al.* 1999). TWIST data were used in regional seismic tomographic imaging of upper mantle wavespeed structure (Sol *et al.* 2002) in an SKS study of mantle anisotropy (Kay *et al.* 1999) and a receiver function study of crustal structure (Angus *et al.* 2009). The tomographic study did not yield evidence for differences between Archaean and Proterozoic mantle wavespeed. In contrast, the splitting study revealed marked differences between the two domains, with null measurements characterizing the Proterozoic coastal areas, while moderate to large splitting was found to parallel Archaean Superior trends.

The HuBLE seismograph networks

Preliminary discussions began in the early 1990s concerning a Hudson Bay Lithospheric Experiment designed to study crust–mantle dynamics beneath Hudson Bay, to determine the reason for this intracratonic basin, and to understand the Precambrian processes that shaped the central Canadian Shield. Four co-ordinated activities were discussed: a network of three-component broadband stations deployed for several years, deep seismic reflection profiling along 600 km profiles, ocean-bottom seismometers and single-component land stations to record the large air-gun array to be used in the profiling. International co-ordination and funding of the marine profiling has not yet been achieved, but the network of three-component broadband stations has now been completed by the Canadian and UK components of HuBLE.

The Geological Survey of Canada began deploying POLARIS (Portable Observatories for Lithospheric Analysis and Research Investigating Seismicity; Eaton *et al.* 2005) around western Hudson Bay in 2004. More stations were deployed over the next three years such that 17 POLARIS stations were operating west and north of Hudson Bay by autumn 2007. The University of Western Ontario added four POLARIS stations in Inuit communities of northern Quebec in summer 2005. An additional 12 POLARIS stations were established in northernmost Ontario, south of Hudson Bay, by the Geological Survey of Canada from 2003 to 2005. All of the POLARIS stations use Güralp CMG-3ESP seismometers and Nanometrics Libra, Trident or Taurus data loggers; most sites are extremely remote, use satellite telemetry for real-time data acquisition and are powered by solar panels (Snyder *et al.* 2013).

The UK component of the HuBLE project was deployed in the summer of 2007 by personnel from the University of Bristol, in collaboration with the Geological Survey of Canada. These 10 stations were situated mainly around the islands of northern Hudson Bay, providing excellent azimuthal coverage around the Bay when combined with the existing POLARIS and a few permanent Canadian National Seismograph Network stations (Fig. 3). Figure 4 shows a completed HuBLE-UK Natural Environment Research Council seismograph station in northern Hudson Bay. Each site was equipped with a Güralp CMG-3TD broadband seismometer, recording at 40 samples per second (sps). Güralp data collection modules were used at the stations, which were powered by up to six solar panels (providing 100–140 W power) and three 100 A h deep-cycle batteries. Each remote site was equipped with an iridium satellite modem that provided access to state-of-health data from the stations. Utilizing modems over the iridium network provides pole-to-pole global coverage of both short message and short data burst services. In the case of the Güralp data collection module, this allowed the UK base-station to access weekly

Downloaded from http://sp.lyellcollection.org/ at University of Aberdeen on November 26, 2014

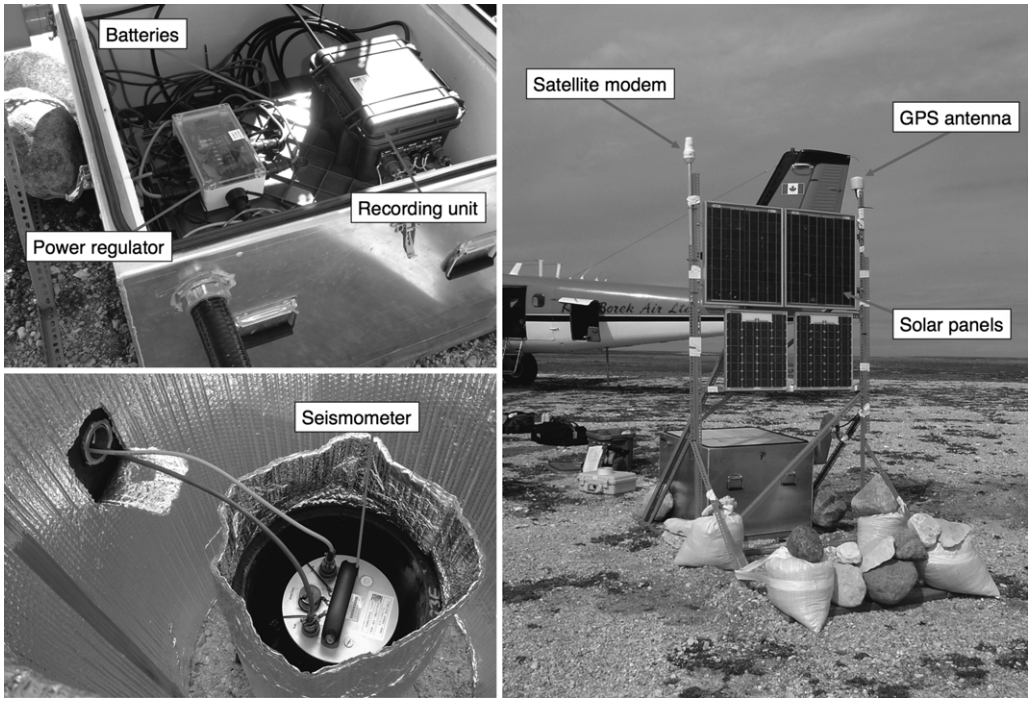

Fig. 4. HuBLE-UK remote station construction. 20–40 W solar panels on a steel frame re-charged 3 × 100 A h batteries that powered the seismometer and recording equipment. The GPS antenna provided continuous accurate timing information for our data. Twice-weekly remote communications with the stations were conducted via the satellite modems. All field equipment were provided by Natural Environment Research Council's seismic equipment pool, SEIS-UK. Modified after Bastow *et al.* (2011*a*).

reports of remote-system state of health. Where problems were diagnosed, low-latency two-way communication for reconfiguration of the remote systems was also utilized via simple terminal interaction. Further details of the UK component of the HuBLE field campaign can be found in Bastow *et al.* (2011*a*).

Nunavut, the homeland of the Inuit, is the most sparsely populated region of Canada, so centres of population and infrastructure are few and far between. Wherever possible, seismograph stations were deployed in secure compounds such as airports and weather stations with mains power supply. Elsewhere, vast tracts of wilderness meant that remote, independently powered recording sites had to be designed. Transportation to these locations was by chartered helicopters or light aircraft with large tundra tyres that permitted landing on relatively flat and well-drained glacial deposits (Fig. 4). Some stations shared logistics with exploration companies by co-location at their camps. All HuBLE-UK stations have now been removed and, with the exception of a few vaults left at airports for potential future re-occupation, no trace of the stations' existence remains at the sites.

HuBLE: the salient results

This section reviews the findings of the major phases of HuBLE. The 'Crustal structure' section presents the crustal studies of Thompson *et al.* (2010) and Pawlak *et al.* (2011, 2012), which adopted receiver function and ambient noise tomographic methods to constrain fundamental parameters such as crustal thickness and seismic wavespeed structure across the Bay region. The 'Seismicity in northern Hudson Bay' section looks at seismicity in northern Hudson Bay and its implications for the state of crustal stress in the region. The section entitled 'Mantle seismic anisotropy: evidence from SKS splitting' reviews the seismic anisotropy studies of Bastow *et al.* (2011*b*) and Snyder *et al.* (2013), who performed shear wave splitting of SKS phases to study mantle anisotropy. The 'Surface wave tomography' section reviews various regional surface wave studies conducted across the Bay region (e.g. Darbyshire 2005; Darbyshire & Eaton 2010; Darbyshire *et al.* 2013). Finally, the section entitled 'Mantle transition zone structure' summarizes the work of Thompson *et al.* (2011), who performed a receiver function study of

Downloaded from http://sp.lyellcollection.org/ at University of Aberdeen on November 26, 2014

the mantle transition zone with a view to improving understanding of its thermal structure.

Crustal structure

Receiver function analysis captures *P*- to *S*-wave conversions that occur at velocity contrasts in the crust and mantle recorded in the *P*-wave coda from distant (teleseismic) earthquakes (Fig. 5a; Langston 1979; Helffrich 2006). The abrupt change in wavespeed usually encountered at the Moho makes receiver function analysis a particularly powerful means of studying the properties of the crust. The arrival-times of *P* to S conversions and subsequent reverberent phases from the Moho can be used to constrain bulk crustal properties: crustal thickness (H) and V_p/V_s ratio (κ) (Zhu & Kanamori 2000). These parameters can be related subsequently to bulk crustal composition via Poisson's ratio (e.g. Christensen 1996). Thompson *et al.* (2010) carried out such a study of crustal structure in northern Hudson Bay, providing for the first time detailed constraints on crustal architecture across the boundaries between many of the tectonic subdivisions that comprise the Canadian Shield.

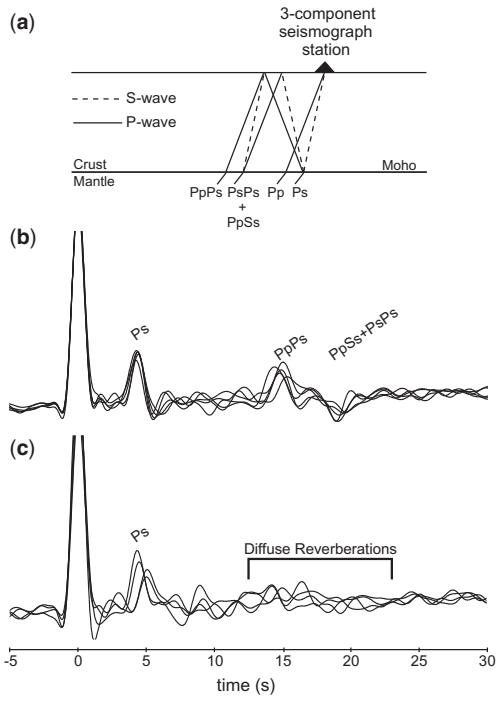

Fig. 5. Receiver functions from the Rae and Hearne domains. (**a**) Ray diagram of phases used in the Hκ analysis. (**b**) Stacked receiver functions for stations in the Palaeoarchaean Rae domain. Note the similarities in Moho Ps (a P-to-S conversion from the Moho) arrivals. (**c**) Stacked receiver functions for stations in the Meso-to-Neoarchaean Hearne domain, where significantly more variable Ps arrival times and amplitudes are seen. The increased complexity of the Moho into the Hearne domain is evident particularly in the reverberated phases, which have lower amplitude and are much less coherent than within the Rae domain. Modified after Thompson *et al.* (2010).

Receiver functions from within the Palaeoarchaean Rae domain reveal remarkably simple crust, with high-amplitude, impulsive Moho conversions and reverberations (Fig. 5b). The crust is also seismically transparent, with little evidence for internal architecture. The Rae domain has the thinnest crust (*c.* 37 km; Fig. 6a) and the lowest V_p/V_s ratios (Fig. 6b; ≤ 1.73) in the region. More northerly stations display slightly thicker crust, up to *c.* 42 km. In contrast to the Rae, the crust and Moho of the Hearne domain crust is more complex (thus making Hκ analysis more challenging), with evidence for internal architecture (Fig. 5c). Crustal thickness within the Hearne is *c.* 38 km and the mean V_p/V_s ratio is *c.* 1.76 (Fig. 6b). Uncertainties in the Thompson *et al.* (2010) study are of the order ± 2 km for crustal thickness, and ± 0.03 for V_p/V_s ratio.

Within the Palaeoproterozoic Quebec–Baffin segment of the THO, bulk crustal properties are more variable than in the neighouring Archaean Hearne and Rae domains. Higher V_p/V_s ratios (>1.75) are found around the Hudson Strait than further north within Baffin Island and further west towards NW Hudson Bay (*c.* 1.73: Fig. 6b). The thickest crust (*c.* 43 km) underlies stations in central and southern Baffin Island (Fig. 6a). Thompson *et al.* (2010) also found evidence, particularly in the northern Rae domain, for a Hales discontinuity in the shallow lithospheric mantle at *c.* 60–90 km depth (Hales 1969).

Ambient-noise tomography uses the cross-correlation of diffuse wavefields (e.g. ambient noise, scattered coda waves) to estimate the Green's function between pairs of seismograph stations (e.g. Shapiro *et al.* 2005). This technique is a popular tool for crustal studies and was particularly useful in the HuBLE project to glean information on crustal structure beneath Hudson Bay. Pawlak *et al.* (2011, 2012) used 21 months of continuous recording at 37 stations around Hudson Bay to measure dispersion characteristics of fundamental-mode Rayleigh wave group velocity. The signals extracted contain preferred azimuths that are indicative of stationary coastal noise sources near southern Alaska and Labrador. Tomographic methods are then used to reconstruct a velocity model that is best resolved in areas of dense, crossing path coverage.

An important feature of the tomographic models is a prominent low-velocity region beneath Hudson Bay (Fig. 7). At mid-crustal depths (i.e. longer

Downloaded from http://sp.lyellcollection.org/ at University of Aberdeen on November 26, 2014

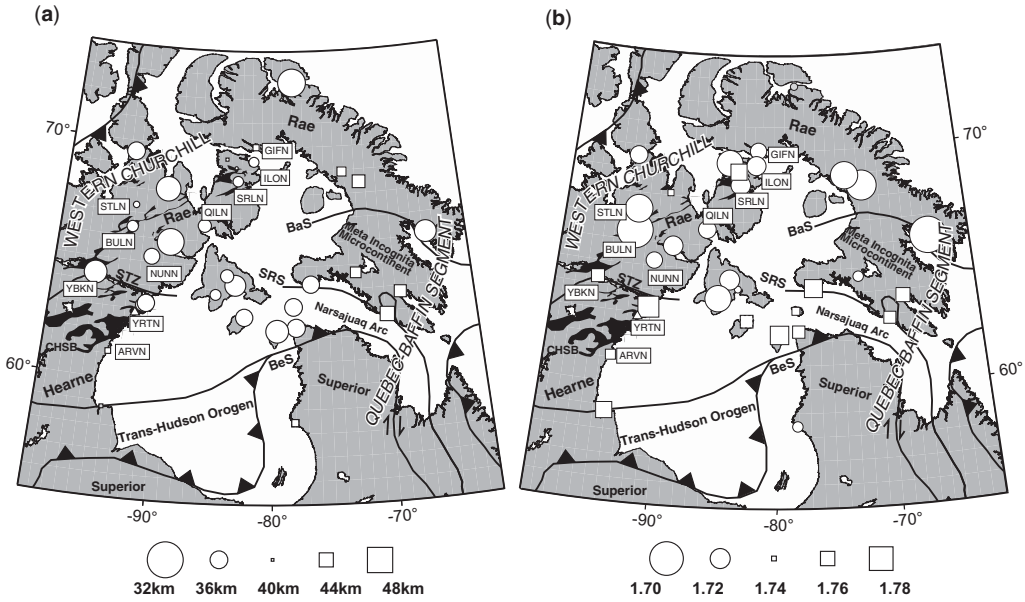

Fig. 6. Crustal thickness (**a**) and V_p/V_s ratio (**b**) in the Hudson Bay region determined using the method of Zhu & Kanamori (2000). Black regions are 2.6–2.7 Ga greenstone belts. BaS, Baffin Suture; BeS, Bergeron Suture; SRS, Soper River Suture. Modified after Thompson *et al.* (2010).

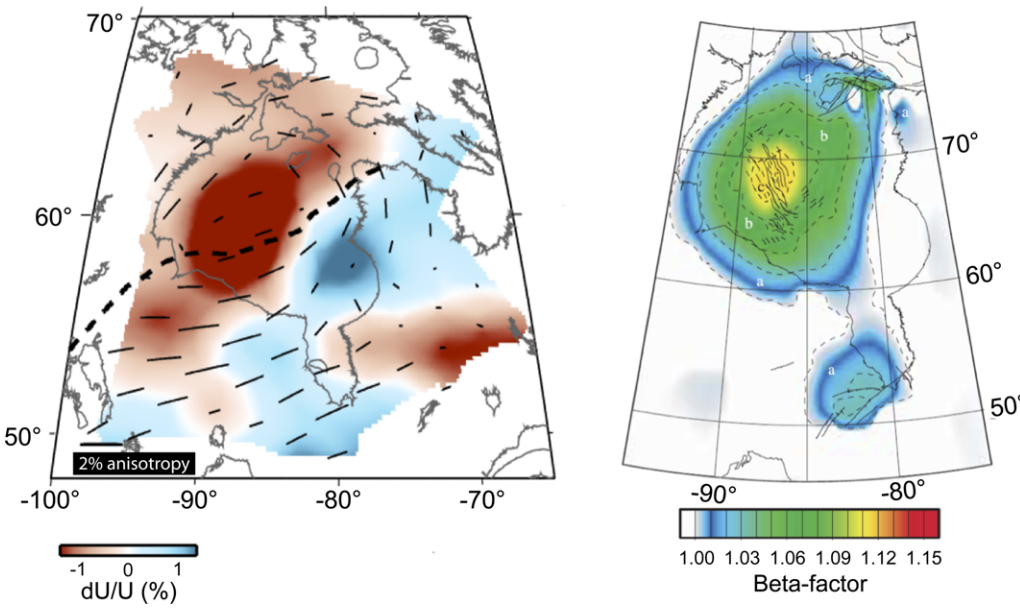

Fig. 7. A comparison of anisotropic tomographic inversion result for 10 s period (left), with the lithospheric stretching factor (β) for the Hudson Bay basin (Hanne *et al.* 2004). The contrast between slow wavespeeds beneath the Trans Hudson Orogen and the neighbouring Archaean Superior craton persists to at least a 40 s period (see Pawlak *et al.* 2011, figs 11 & 12). Modified after Pawlak *et al.* (2011, 2012).

Downloaded from http://sp.lyellcollection.org/ at University of Aberdeen on November 26, 2014

periods than shown in Fig. 7), the Pawlak *et al.* (2011) study reveals that fundamental-mode Rayleigh velocity within the Superior craton (3.18 ± 0.03 km s^{-1}) is significantly greater than the velocity within the Trans Hudson Orogen beneath Hudson Bay (3.10 ± 0.03 km s^{-1}). Rayleigh-wave anisotropy inferred from azimuthal analysis of ambient noise (Pawlak *et al.* 2012) reveals an arcuate pattern of fast directions interpreted to be indicative of the double-indenter geometry of the Superior craton. At most periods, their results suggest a significant change in anisotropic direction across the inferred primary suture beneath Hudson Bay. The region of lowest velocity beneath Hudson Bay (Fig. 7) corresponds remarkably well with the pattern of lithospheric stretching proposed by Hanne *et al.* (2004): *c.* 3 km of crustal thinning.

Seismicity in northern Hudson Bay

Northern Hudson Bay is a region of moderate intraplate seismicity, mainly within the Boothia Uplift–Bell Arch structure (Basham *et al.* 1977), where earthquakes up to $Mw = 6.2$ have been documented. Using data from the HuBLE network, focal mechanisms for five moderate earthquakes in the time period 2007–2009 have been determined by fitting surface waveforms (Fig. 8: Steffen *et al.* 2012). These small earthquakes, of depth 3–17 km, have thrust-fault mechanisms, consistent with previously determined focal mechanisms for this region as well as model predictions for glacial isostatic adjustment. Steffen *et al.* (2012) performed a stress inversion using available focal mechanisms and found a maximum compressive stress direction, SH_{max}, oriented approximately NNW–SSE. This orientation is surprising, as it is rotated by about 90° from previous glacial isostatic adjustment model estimates, which assume a background stress field in North American with SH_{max} oriented NE–SW. These results indicate that existing crustal fault zones exert a strong influence on the local stress field.

Mantle seismic anisotropy: evidence from SKS splitting

Seismic anisotropy – the directional dependence of seismic wavespeed – can be measured from the waveforms of teleseismic earthquakes via analysis of shear-wave splitting (e.g. Silver & Chan 1991). When a horizontally polarized shear wave, such as SKS, enters an anisotropic medium it will split into two orthogonally polarized waves. Splitting

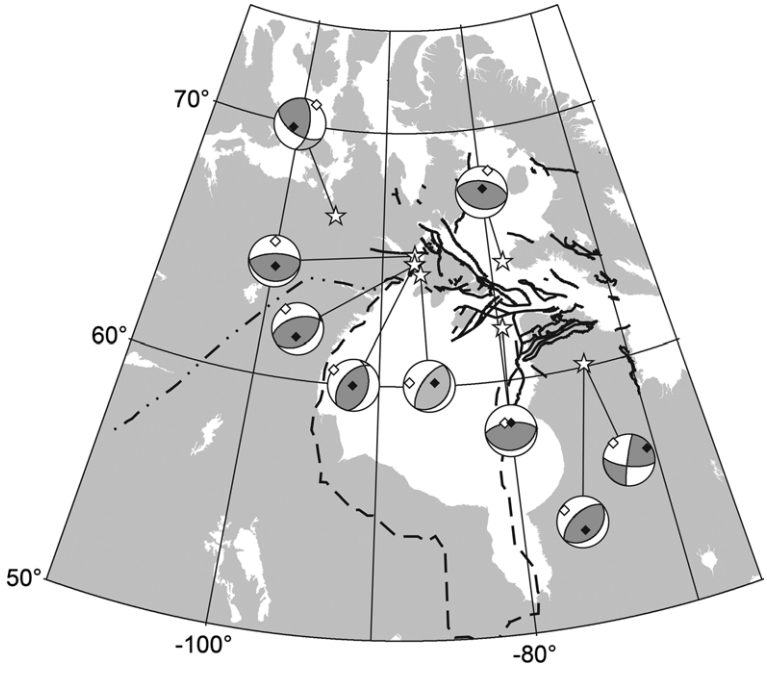

Fig. 8. Focal mechanisms for earthquakes between 2007 and 2009 and from studies that predate HuBLE (grey). Solid black lines show faults; the dashed line shows the Phanerozoic zero edge; the dashed–dotted line shows the Snowbird Tectonic Zone. After Steffen *et al.* (2012).

Downloaded from http://sp.lyellcollection.org/ at University of Aberdeen on November 26, 2014

can be quantified by the time delay (δt) between the two shear waves, and the orientation (φ) of the fast shear wave. These splitting parameters can subsequently be used to understand the preferential alignment of minerals in the crust and/or mantle, or the preferential alignment of fluid or melt (e.g. Blackman & Kendall 1997). Many processes can lead to such anisotropy, including flow of the asthenosphere parallel to absolute plate motion (e.g. Bokelmann & Silver 2002; Assumpção *et al.* 2006), mantle flow around deep continental keels and slabs (e.g. Fouch *et al.* 2000; Di Leo *et al.* 2012), and a pre-existing fossil anisotropy frozen in the lithosphere (e.g. Bastow *et al.* 2007). Bastow *et al.* (2011*b*) and Snyder *et al.* (2013) used shear wave splitting of SKS phases at HuBLE and POLARIS stations in the Hudson Bay region to infer patterns of seismic anisotropy in the Laurentian crust and mantle (Fig. 9).

In the northern part of Hudson Bay, Bastow *et al.* (2011*b*) found no significant variation in splitting parameters at most stations across the HuBLE network. One exception was permanent station FRB on Baffin Island, for which more than a decade of data were available. Here, significant back-azimuthal variation in φ and δt was found, raising the possibility that complex patterns of anisotropy exist beneath the region (Fig. 10). In a parallel analysis of SKS splitting, Snyder *et al.* (2013) proposed that two layers of anisotropy exist beneath the Bay, one paralleling near-surface tectonic trends and an underlying fabric paralleling present-day plate motion.

Surface wave tomography

Studies of fundamental-mode Rayleigh wave dispersion were carried out for two-station paths across the Hudson Bay region by Darbyshire & Eaton (2010). The dispersion curves clearly indicated a thick, fast lithospheric keel beneath the region, with phase velocities significantly greater than those associated with global reference models. The phase velocities were also systematically higher than the Canadian Shield average (Brune & Dorman 1963), corroborating global tomographic models that place the centre of the high-wavespeed lithospheric keel beneath Hudson Bay (e.g. Nettles & Dziewonski 2008). Each two-station dispersion curve was inverted for a 1D shear wavespeed profile representing the average structure along the inter-station path. The period ranges recovered from the dispersion analysis allowed for reliable models from lower-crustal depths (*c.* 35–40 km) to mantle depths of *c.* 300 km. Each path-averaged model showed a prominent high-wavespeed anomaly, interpreted as the lithospheric 'lid' in the upper mantle.

Different proxies for lithospheric thickness exist in the literature because fundamental-mode

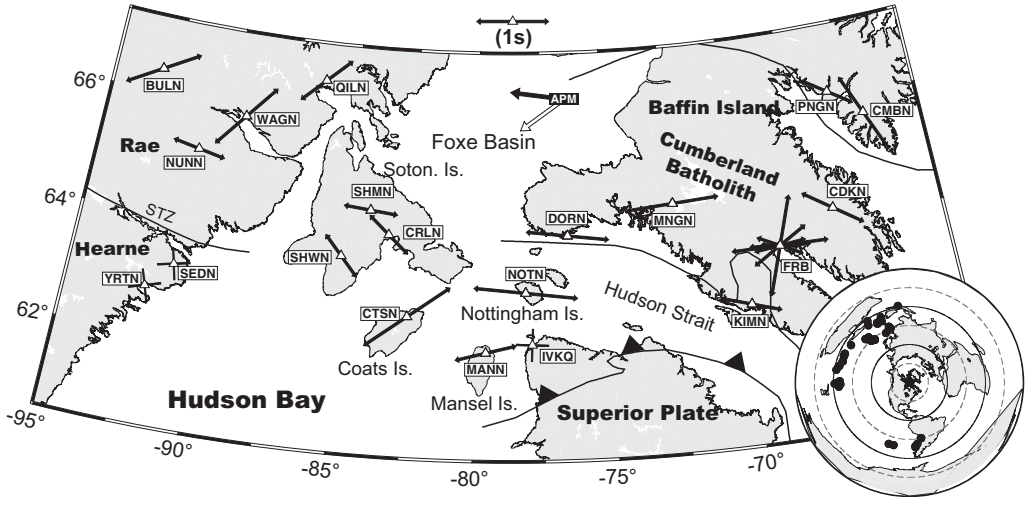

Fig. 9. Shear wave splitting parameters (arrows) and null results (solid lines) from HuBLE-UK and neighbouring POLARIS stations (triangles) in northern Hudson Bay from the study of Bastow *et al.* (2011*b*). STZ, Snowbird Tectonic Zone. Solid black lines are sutures. B.S., Baffin Suture. Inset: Back-azimuth and distance distribution of earthquakes used in study. Concentric circles indicate 30° intervals from centre of network at 75°W, 63°N. APM-absolute plate motion from the HS3-Nuvel-1A model (Gripp & Gordon 2002) in both hotspot reference frame (white APM arrow) and no-net rotation reference frame (black APM arrow).

Downloaded from http://sp.lyellcollection.org/ at University of Aberdeen on November 26, 2014

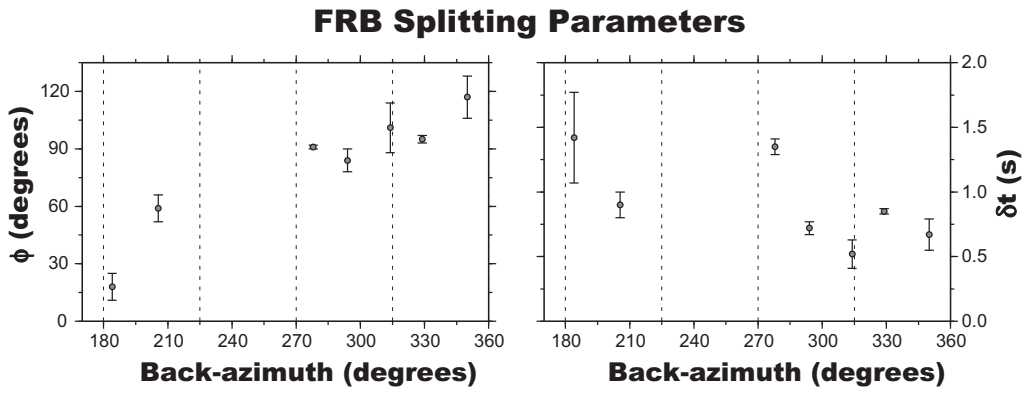

Fig. 10. Shear wave splitting parameters at permanent Canadian National Seismograph Network station FRB (Fig. 9). Back-azimuth dependence of φ and δt might be the result of a dipping layer of anisotropy beneath Baffin Island. Back-azimuthal variations in splitting parameters could also result from multiple layers of seismic anisotropy beneath the region (e.g. Snyder *et al.* 2013). Modified after Bastow *et al.* (2011*b*).

surface wave models are essentially insensitive to first-order discontinuities (see e.g. Eaton *et al.* 2009). In some studies, negative gradients in the models are used, although these can be difficult to constrain. Other authors choose (somewhat arbitrarily) a contour of positive V_s anomaly with respect to the global reference (e.g. PREM, ak135). The 1.5–2.0% anomaly range is commonly used (see Darbyshire & Eaton (2010) for a more detailed discussion). Using a proxy based on the depth to the 1.7% fast anomaly, the depth to the base of the lithosphere was interpreted to vary from *c.* 190 km beneath the Hudson Strait area to at least 240–280 km beneath central Hudson Bay. Within the lithospheric lid, maximum seismic wavespeed anomalies varied from *c.* 4 to 7%, which is fast relative to the global reference (Fig. 11).

The lithosphere–asthenosphere boundary depth variations inferred from the surface-wave analysis, and from interpretation of previous studies in the Canadian Shield, indicate that the lithosphere is thickest beneath central Hudson Bay (and significantly thicker than in the Superior craton to the south). There appeared to be no spatial correlation between lithospheric thickness, path-averaged seismic wavespeed anomalies and surface ages (Archaean v. Proterozoic). This result is similar to interpretations of the Fennoscandian (Bruneton *et al.* 2004) and Australian (Simons *et al.* 1999; Fishwick *et al.* 2005) lithosphere, but contrasts with systematic changes in lithospheric thickness between Archaean and Proterozoic domains in central Asia (Lebedev *et al.* 2009) and southern Africa (Li & Burke 2006).

The dispersion curves from a total of 172 interstation paths across the Hudson Bay region were combined in a tomographic inversion by Darbyshire *et al.* (2013), solving simultaneously for isotropic phase velocity heterogeneity and azimuthal anisotropy. The resulting phase velocity maps were subsequently used as the basis for a full 3D model of shear wave velocity and anisotropy beneath the region (Fig. 12). The model confirmed the earlier findings of a thick, fast lithospheric keel, but highlighted internal velocity variations and stratification of seismic anisotropy within the cratonic lithosphere.

In the uppermost mantle, probably associated with the intracratonic basin, seismic velocities immediately beneath the Bay are relatively low compared with those beneath the surrounding Archaean landmass, and anisotropic fast directions wrap around the Bay. In contrast, in the 70–160 km depth range, the model shows two high-velocity cores beneath the central Superior and Churchill cratons, separated by a near-vertical curtain of lower-velocity material. In this depth range, no large-scale coherency in anisotropic pattern is evident. In contrast, the model also images a basal lithospheric layer with a significantly more homogeneous velocity structure than the mid-lithosphere. Anisotropy within this layer is coherent, with a pattern strongly reminiscent of the inferred geometry of the THO structure (Darbyshire *et al.* 2013).

Mantle transition zone structure

The seismic discontinuities observed at depths of *c.* 410 and 660 km define the mantle transition zone (TZ), and are commonly attributed to phase transitions in the olivine system (olivine to wadsleyite, the '410', and ringwoodite to perovskite + magnesiowüstite, the '660', respectively; Bina & Wood 1987; Helffrich 2000; Ita & Stixrude 1992).

Downloaded from http://sp.lyellcollection.org/ at University of Aberdeen on November 26, 2014

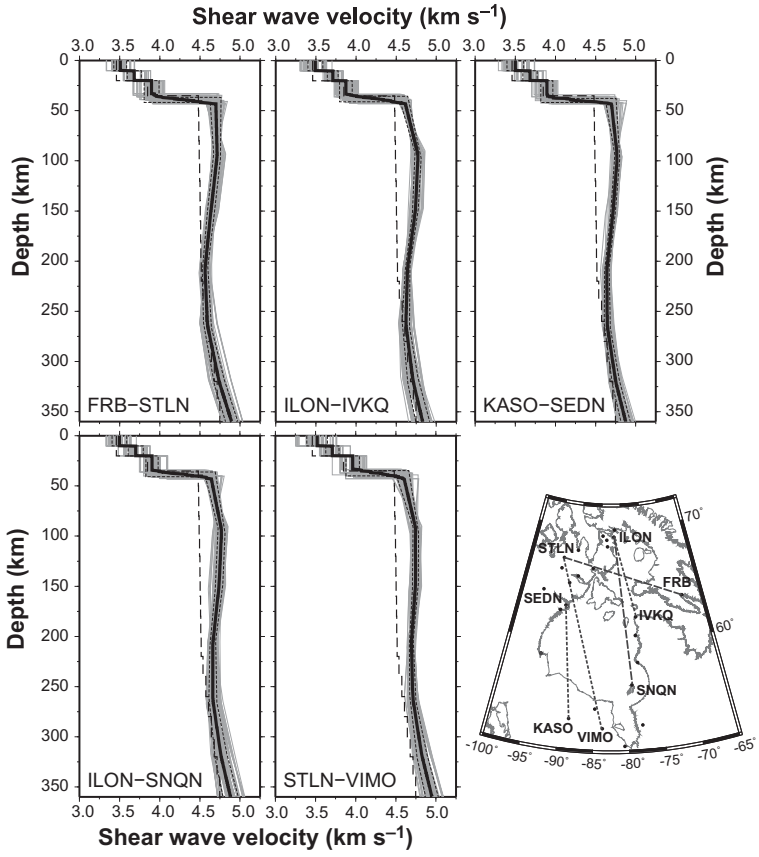

Fig. 11. One-dimensional shear wave velocity profiles for selected paths across Hudson Bay derived from surface wave dispersion. Grey lines are individual model solutions in the Monte-Carlo modelling scheme; the mean and 1 standard deviation bounds of the ensemble are solid black and dotted black lines, respectively. The black dashed line is the ak135 global reference model. Inset: inter-station paths and station names. Modified after Darbyshire & Eaton (2010).

Described by their Clapeyron slopes, the '410' and '660' will vary in depth if temperature conditions are varied. The opposite Clapeyron slopes of these discontinuities result in a thickened transition zone in cold regions; hot regions will act to thin it (e.g. Helffrich 2000). By analysing the nature of transition zone seismic discontinuities using receiver function analysis, Thompson *et al.* (2011) explored the thermal and chemical state of the mantle beneath the Hudson Bay region.

Thompson *et al.* (2011) showed that, beneath a significant portion of cratonic North America, the TZ seismic discontinuities are unperturbed compared with the global mean, with the implication that there is no seismically detectable thermal variation at TZ depths beneath one of the deepest and most laterally extensive continental keels on the planet (Fig. 13).

A new relative arrival-time upper mantle tomographic model for northern Hudson Bay

Overview

Using teleseismic data recorded by HuBLE and surrounding POLARIS seismograph stations since 2007 a new study of *P*-wave mantle velocity structure using least-squares tomographic inversion of relative arrival-times is presented using the method of VanDecar *et al.* (1995). Body wave tomographic methods such as this benefit from particularly good lateral resolution of velocity anomalies. The study thus presents an excellent opportunity to examine whether variations in seismic wavespeed exist between Phanerozoic and Archaean mantle juxtaposed during the THO. This study, which samples

Downloaded from http://sp.lyellcollection.org/ at University of Aberdeen on November 26, 2014

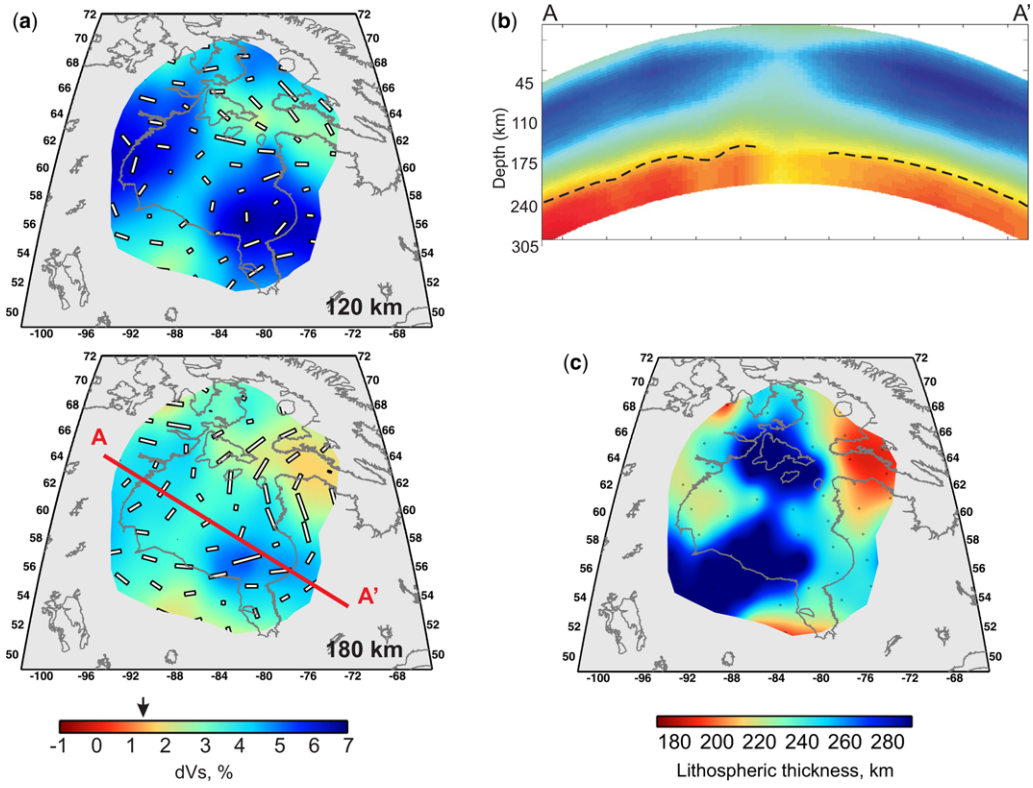

Fig. 12. (**a**) Depth slices through the anisotropic surface-wave tomographic model of Darbyshire *et al.* (2013). The colour scale represents the percentage deviation of shear wavespeed from the iasp91 global reference model and the pale yellow bars indicate the direction and relative strength of azimuthal anisotropy across the region. The arrow on the colour scale shows the 1.7% positive wavespeed anomaly used as a proxy for the base of the seismological lithosphere ('LAB'). (**b**) Cross-section through profile A–A′ of the tomographic model. The black dashed line shows the inferred depth to the 'LAB' proxy. (**c**) Lithospheric thickness across the Hudson Bay region inferred from the tomographic model, using the 1.7% 'LAB' proxy.

only Precambrian geology, is particularly valuable because most studies of cratons using the method include data from stations deployed within younger (Phanerozoic) terranes. In Tanzania, for example, the high wavespeed Tanzania craton contrasts with the neighbouring East African Rift (Ritsema *et al.* 1998). In SE Canada, the high wavespeed Superior craton contrasts with lower wavespeeds associated with the Phanerozoic Great Meteor Hotspot and Appalachian terranes (e.g. Eaton & Frederiksen 2007; Frederiksen *et al.* 2007; Villemaire *et al.* 2012). In contrast, the major anomalies illuminated in this study will probably be older than *c.* 1.8 Ga. After presenting the results of this new tomographic study, these new constraints are discussed in light of other tomographic studies in the region that used complementary methods such as surface wave dispersion (e.g. Darbyshire & Eaton 2010).

Method of relative arrival-time determination

Manual picking of the first arriving *P*-wave phase identifiable across the seismograph network was performed on waveforms that were filtered with a zero-phase two-pole Butterworth filter with corner frequencies 0.4–2 Hz. Subsequently, phase arrivals and relative arrival-time residuals were more accurately determined using the multi-channel cross-correlation technique (MCCC) of VanDecar & Crosson (1990); we selected a 3 s window containing the initial phase arrival and typically one or two cycles of *P*-wave energy to cross-correlate. The chosen bandwidth is similar to that used in other teleseismic tomographic studies in both tectonically active (e.g. Bastow *et al.* 2008) and shield (e.g. Frederiksen *et al.* 2007) regions. The filter bandwidth is designed to retain as high a

Downloaded from http://sp.lyellcollection.org/ at University of Aberdeen on November 26, 2014

frequency as possible since our inversion procedure adopts ray theory (the infinite frequency approximation). All waveforms with cross-correlation coefficients <0.85 were eliminated from the analysis.

The MCCC method also provides a means of quantifying the standard error associated with each arrival time. In this study relative arrival times determined in this way have mean standard deviation of 0.02 s. In line with other studies using the MCCC method (Tilmann *et al.* 2001; Bastow *et al.* 2005), we regard the MCCC-derived estimates of timing uncertainty as optimistic.

Relative arrival-time residuals t_{RES} for each station are given by:

$$t_{\mathrm{RESi}} = t_{\mathrm{i}} - (t_{\mathrm{ei}} - t_{\mathrm{e}}), \qquad (1)$$

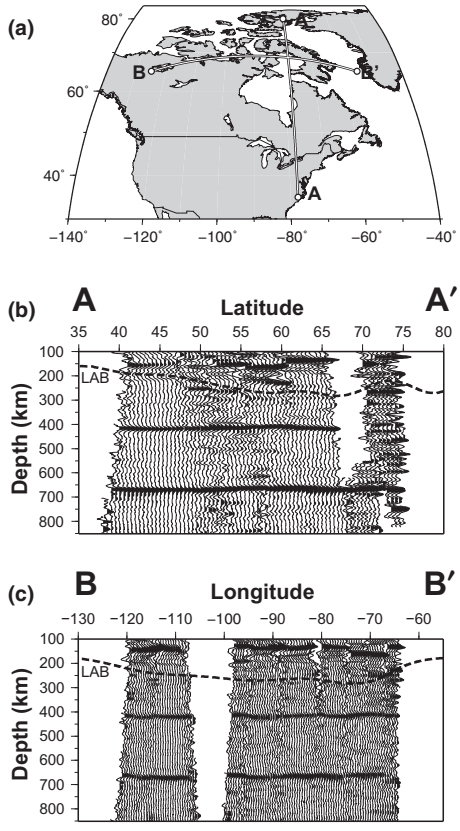

Fig. 13. (**a**) The orientation of two receiver function transects plotted in (b) and (c). (**b**) A north–south transect through 78°W showing the 1.0 Hz migrated data (S40RTS corrected). The dashed black line is the +1.75% contour, sometimes chosen as a proxy for lithospheric thickness (Fig. 2b). (**c**) Corresponding east–west transect showing same data as the north–south transect. Modified after Thompson *et al.* (2011).

where t_{i} is the relative arrival time for each station i; t_{ei} is the expected travel time based on the IASP91 travel time tables (Kennett & Engdahl 1991) for the ith station; and t_{e} is the mean of the IASP91 predicted travel times associated with that particular event. The final travel time dataset comprises 3682 *P*-wave travel times (Fig. 14).

Analysis of travel-time residuals

International Seismological Catalogue travel-time data for permanent station FRB (Fig. 15) in Iqaluit, Baffin Island (Fig. 3) show that the mean absolute delay time with respect to the IASP91 travel-time tables for *P*-wave arrivals is amongst the earliest of all permanent stations; mantle seismic wave-speeds beneath FRB are therefore amongst the fastest worldwide (Poupinet 1979). All *P*-wave velocity anomalies shown in this tomographic study should thus be considered markedly fast compared with normal mantle, with red low-velocity regions slower and blue high-velocity regions faster than the background mean of the shield, not the global average.

Model parameterization and inversion procedure

Upper mantle wavespeed structure is imaged using regularized, least-squares inversion of Canadian relative arrival-time residuals following the method of VanDecar *et al.* (1995). The parameterization

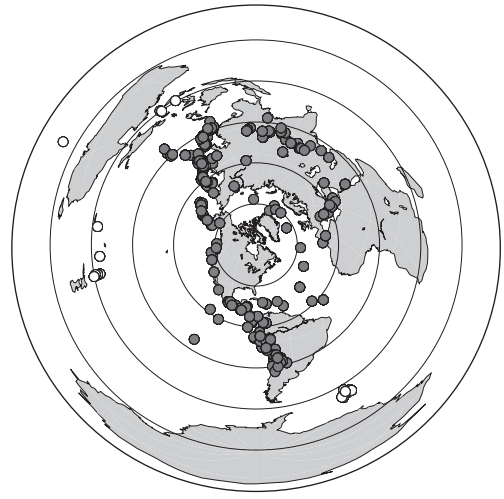

Fig. 14. Back-azimuth and distance distribution of earthquakes used in study. Concentric circles indicate 30° intervals from centre of network at 75°W, 63°N. Dark grey dots are direct *P*-arrivals; white dots are core phases (e.g. PKP).

Downloaded from http://sp.lyellcollection.org/ at University of Aberdeen on November 26, 2014

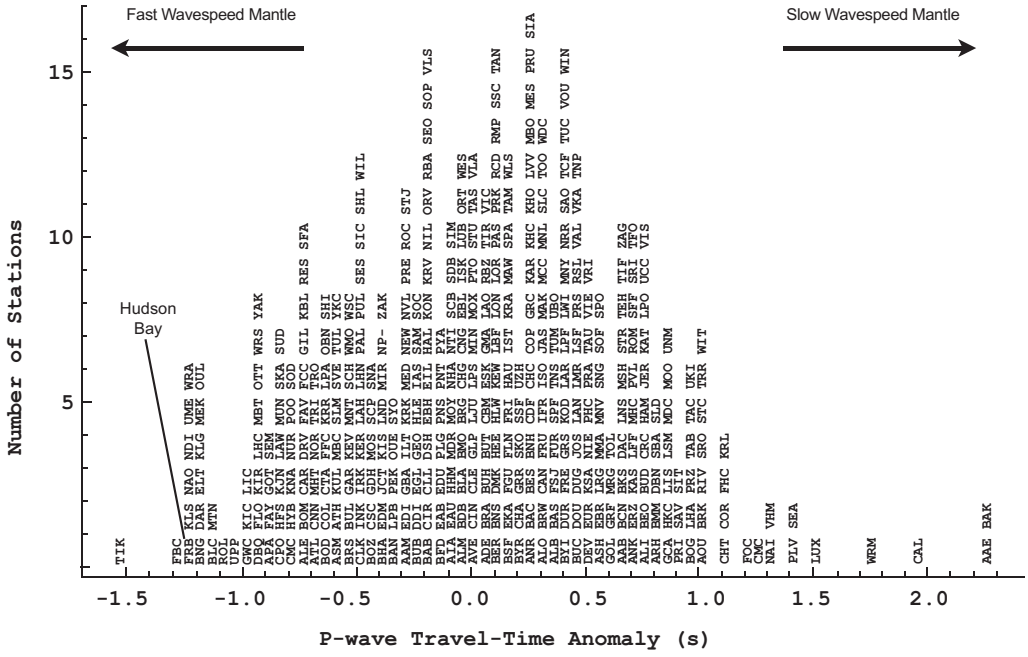

Fig. 15. *P*-Wave travel-time delays for permanent seismograph stations. Note the extremely early arrivals at station FRB in Iqaluit. Modified after Poupinet (1979).

scheme consists of 23 knots in depth between 0 and 1800 km, 50 knots in latitude between 50 and 78°N and 85 knots in longitude between 46 and 114°W: a total of 97 750 knots parameterizing slowness. Knot spacing is 35 km in the innermost resolvable parts (58–71°N, 63–100°W, 0–350 km depth). Outside this region, knot spacing increases to 50 km between 350 and 500 km, to 100 km between 500–1000 km, and then to 200 km at 1800 km depth. Structural interpretations are thus limited to features of spatial wavelength $\geq$70 km in the upper part of the model.

The parameterization scheme continues outside the area of interest so that an unwarranted and spurious structure is not mapped into the region where structural interpretations will be made: an Occam's Razor approach (VanDecar *et al.* 1995). In the regularized least-squares inversion procedure, slowness perturbations, source terms and station terms are determined simultaneously (VanDecar *et al.* 1995). The source terms are free parameters used in the inversion procedure to account for small variations in back-azimuth and incidence angle caused by distant heterogeneities and source mis-locations. The station terms account for travel-time anomalies associated with the region directly beneath the station where the lack of crossing rays prevents the resolution of crustal structure. Since the inverse problem is under-determined (more unknowns than observations), even in the absence of errors, a unique solution cannot be found. A model is therefore chosen that contains the least amount of structure necessary to satisfy the arrival-time data (e.g. Constable *et al.* 1987).

By investigating the trade-off between the root mean square (RMS) residual reduction (the percentage difference between the initial and final RMS misfit to the travel-time equations) and RMS model roughness, a preferred model is selected that fits the data well but does not account for more relative arrival-time residual reduction than can be justified by the *a priori* estimation of data noise levels. All models in this study account for 95% (from 0.384 to 0.02 s) of the RMS of the relative arrival-time residuals. Estimates of RMS timing uncertainty (0.02 s) are thus treated as optimistic bounds when fitting the data. Subtracting the station terms from the delay times reduces the RMS of the relative arrival-time residuals from 0.384 to 0.369 s; these corrected residuals reflect more accurately the proportion of the delay-time anomalies that will be mapped into the region of the model where tectonic interpretations are drawn.

Resolution

The resolving power of the inversion technique in this study is assessed by analysing the ability of

Downloaded from http://sp.lyellcollection.org/ at University of Aberdeen on November 26, 2014

the ray geometry to retrieve a checkerboard model using raypaths through a 1-D Earth. In the checkerboard test, positive and negative slowness-anomaly ($V_p = \pm 5\%$) spheres described by Gaussian functions across their diameter are placed in two layers at 175 and 400 km depth (Fig. 16a, b). The checkerboard approach permits assessment of model sensitivity by highlighting areas of good ray coverage, and the extent to which smearing of anomalies occurs. These synthetic velocity structures are inverted to use identical model parameterization and inversion regularization as during the inversion of the observed data. A Gaussian residual time error component with a standard deviation of 0.02 s is added to the theoretical *P*-wave travel times (the standard deviation of noise estimated for the observed data). Lateral resolution of the anomalies in Figure 16b and c is good, with *c.* 30% amplitude resolution not uncommon in regularized, under-determined tomographic inversions such as this. Vertical resolution is good in some parts of the model (e.g. beneath the central Rae domain; Fig. 16e), but moderate in others. For example, vertical smearing in areas such as southern Baffin Island (Fig. 16f) is considerable, meaning that the model cannot be used to place tight depth constraints on wavespeed variations.

The HuBLE P-wave velocity model

Cross sections and depth slices through the new *P*-wave velocity model are shown in Figure 17. Depth sections at lithospheric depths (Fig. 17a, b) indicate relatively little heterogeneity, with peak-to-peak amplitudes of $<1\%$. This compares with peak-to-peak anomalies of *c.* 3% in active areas such as the Ethiopian Rift (e.g. Bastow *et al.* 2005). Across the Snowbird Tectonic Zone (Rae–Hearne boundary), for example, there is almost no discernible variation in seismic wavespeed (Fig. 17a, b, e), although it is acknowledged that this could be partly the result of poor resolution at the edge of the model (Fig. 16b).

One area where relatively strong variations in seismic wavespeed can be observed is the Quebec–Baffin segment of the THO (Fig. 17a, b, e). Here, fast wavespeeds associated with the southern edge of the Churchill plate (i.e. Baffin Island) contrast with slower wavespeeds beneath the Baffin Strait, with a subvertical to south–north-dipping boundary between the two (Fig. 17e). This region corresponds to a region of active seismicity and Palaeozoic faulting (e.g. Steffen *et al.* 2012). The depth extent of the low-wavespeed anomaly beneath the Baffin Strait (Fig. 17e) is *c.* 300 km, implying that it may extend through most or all of the lithosphere (allowing for a finite amount of vertical smearing in the model; Fig. 16). It must be noted, however, that resolution in this part of the velocity model is moderate: amplitude recovery is low and vertical smearing is clearly evident in the resolution tests (Fig. 16).

Discussion

Causes of seismic heterogeneity in tomographic models

A number of factors can affect seismic velocity in the mantle, including temperature, partial melt and composition (Karato 1993; Goes *et al.* 2000; Goes & van der Lee 2002). Variations in seismic anisotropy may be manifest as velocity heterogeneities. However, temperature is often cited as the main source of mantle heterogeneity in the upper mantle (e.g. Goes & van der Lee 2002).

The markedly fast wavespeeds observed in global and continent-scale tomographic images of the Canadian Shield mantle indicate strongly that the lithosphere beneath the Hudson Bay region is cold relative to the global average (e.g. Darbyshire *et al.* 2007; Nettles & Dziewonski 2008; Darbyshire & Eaton 2010). Composition is also an important contributing factor, however: shields are generally associated with cold, depleted, mechanically strong mantle material characterizing their tectospheric 'roots' (e.g. Jordan 1978). It is often commonly assumed that the Archaean cores of the continents are characterized by the seismically fastest and thickest lithosphere on Earth, with thinner and slower wavespeed structure characterizing Proterozoic regions (Durrheim & Mooney 1994). More recent seismic studies of mantle structure in Australia (Simons *et al.* 1999; Fishwick *et al.* 2005; Fishwick & Reading 2008), Canada (Darbyshire & Eaton 2010) and Fennoscandia (e.g. Bruneton *et al.* 2004) question this simple correlation between surface geology age and underlying mantle structure and we revisit this issue in the 'Implications for the formation of the Laurentian keel' section.

As indicated in the 'Analysis of travel-time residuals' section, when interpreting tomographic images derived from relative arrival-time data (Fig. 17), it is essential to appreciate the background velocity structure of the region, which is represented in the tomographic images by the $\delta V_p = 0\%$ contour. Studies of Precambrian lithosphere commonly include data from Phanerozoic terranes as well (e.g. Tanzania: Ritsema *et al.* 1998; SE Canada: Villemaire *et al.* 2012). These models illuminate high-/low-velocity anomalies that are sometimes genuinely fast/slow compared with the global mean. However, our study area's mean wavespeed structure is all fast compared with the global average (Fig. 15), with no stations lying off-shield. Both

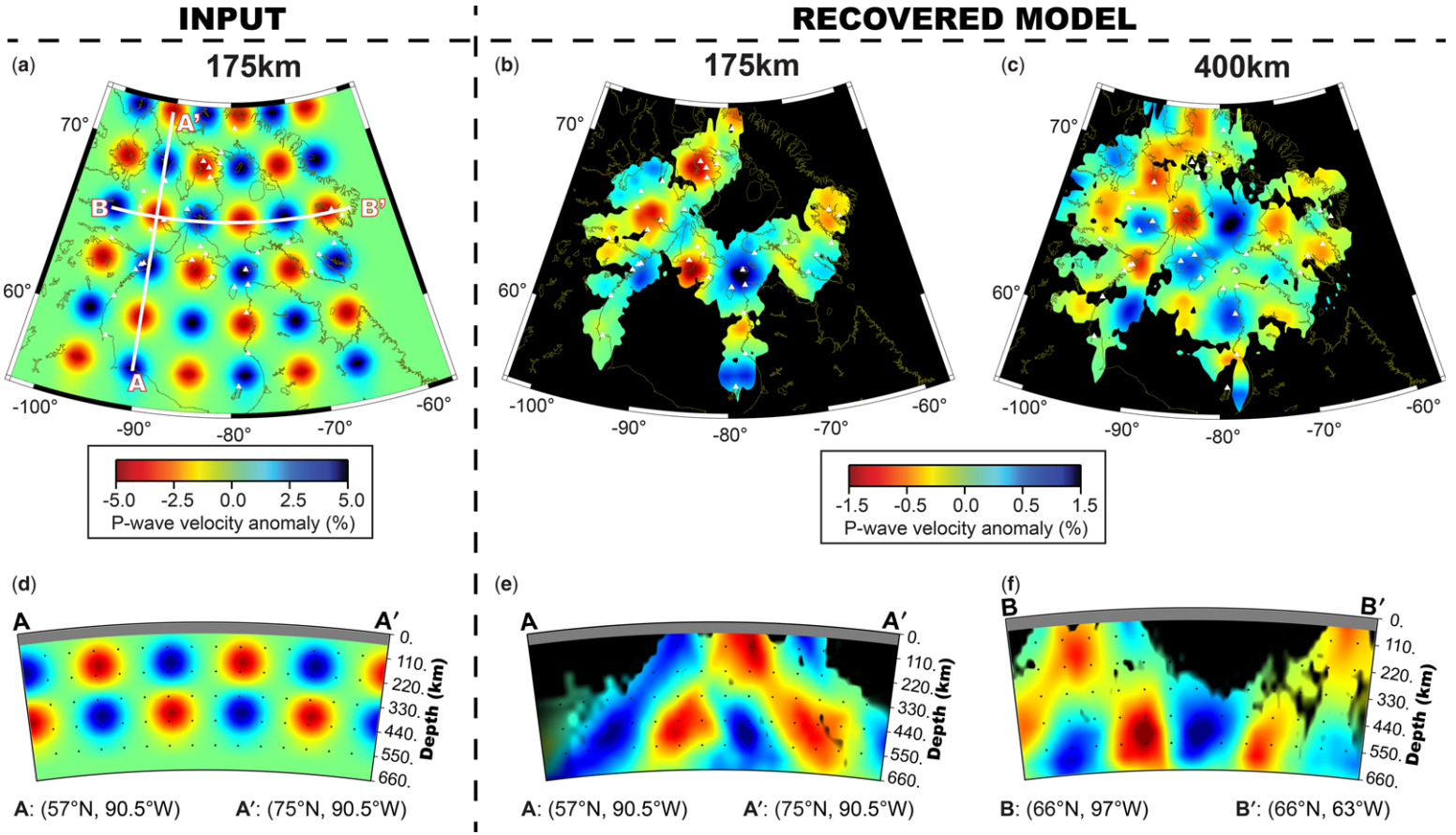

Fig. 16. (**a**, **d**) 175 km depth slice and cross-section through the synthetic checkerboard model. Spheres of diameter 90 km (defined by Gaussian functions across their diameter) of $\delta V_P = \pm 5\%$ peak anomaly are distributed in layers of depth 175 and 400 km in order to simulate relatively short length-scale velocity heterogeneity in the uppermost mantle beneath the study area. (**b**, **c**) Depth slices through the retrieved checkerboard model at 175 and 400 km depth. (**e**, **f**) Cross-sections through the retrieved checkerboard model. The grey bands at the top of the cross-sections preclude the view of the uppermost unresolved part of the model where ray paths are almost all parallel and vertical. Areas of low ray-density (fewer than 10 rays per 30 km^3) are black. Note the different colour scales used in (a) and (d) compared with (b), (c), (e) and (f).

Downloaded from http://sp.lyellcollection.org/ at University of Aberdeen on November 26, 2014

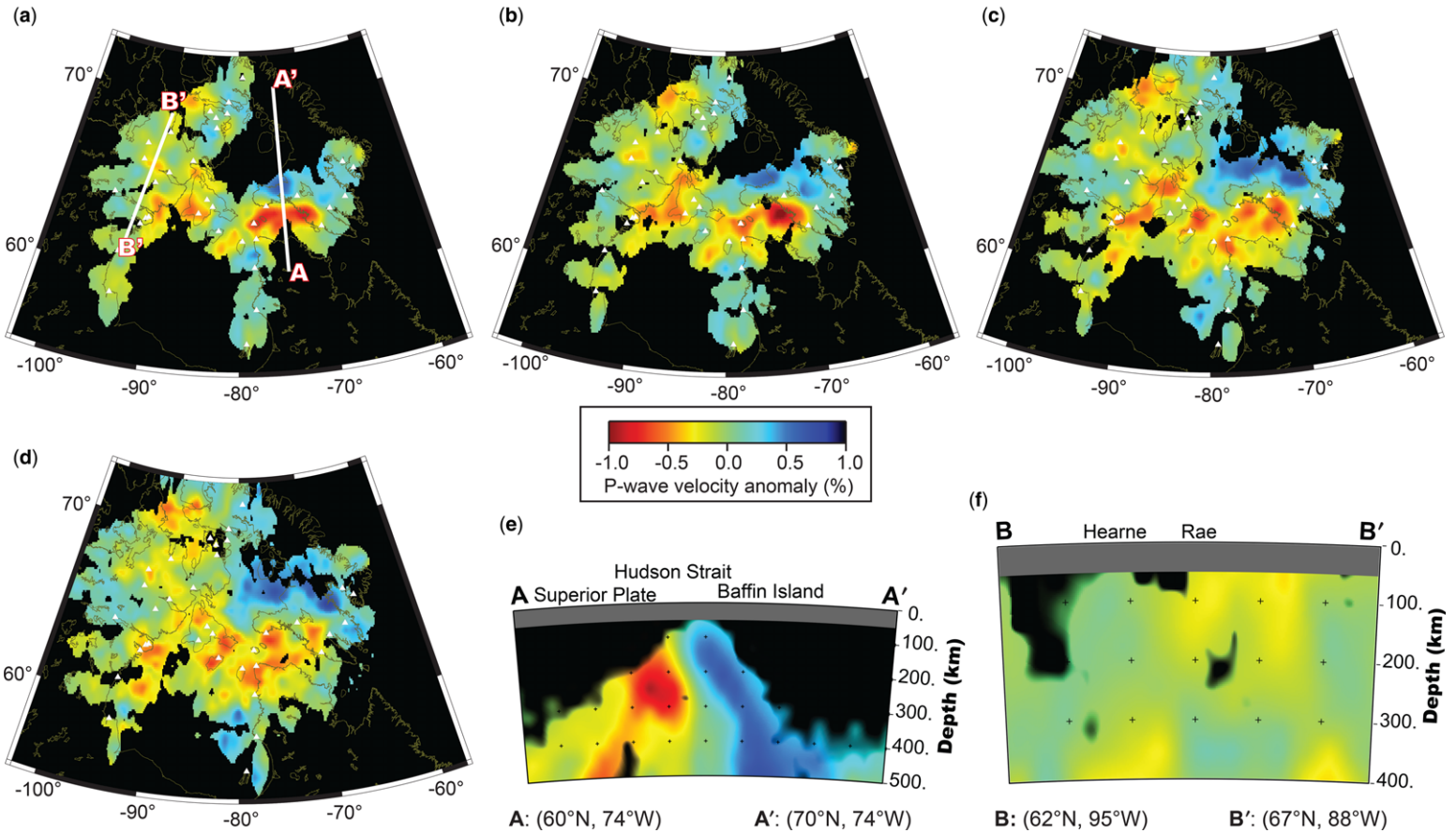

Fig. 17. Depth slices through the *P*-wave velocity model at (**a**) 175 km, (**b**) 250 km, (**c**) 350 km and (**d**) 400 km. (**e** and **f**) Cross-sections through the *P*-wave velocity model. Areas of low ray-density (fewer than 10 rays per 30 km^3) are black.

Downloaded from http://sp.lyellcollection.org/ at University of Aberdeen on November 26, 2014

Downloaded from http://sp.lyellcollection.org/ at University of Aberdeen on November 26, 2014

'low'- and 'high'-velocity anomalies presented in Figure 17 are thus fast compared with the global mean.

The *c.* 1.8 Ga elapsed since the last major tectonic event (the THO) means that lithospheric thermal anomalies associated with magmatism in the region will have long since dissipated. The velocity anomalies in Figure 17 imaged are thus probably sensitive to variable composition across the network.

Implications for the assembly of the Canadian Shield: evidence for modern-style plate tectonics?

Whether or not modern-style plate tectonics operated throughout Precambrian times is debated: its onset has been estimated to be as early as the Hadean (e.g. Hopkins *et al.* 2008) or as late as *c.* 1 Ga (e.g. Stern 2005) – a time span of approximately two-thirds of Earth history (Fig. 1). At crustal depths, the receiver function study of Thompson *et al.* (2010) revealed that crustal character has a strong age dependence, with the implication that crustal formation processes have evolved over time.

The low bulk crustal V_p/V_s ratios of the Palaeoarchaean Rae domain crust (Fig. 6b) are indicative of felsic-to-intermediate composition to rocks in the mid to lower crust (e.g. Christensen 1996). Crustal formation hypotheses involving island arc accretion are thus not easily applied to the Rae domain because arcs are believed to have a basaltic bulk composition (Rudnick 1995). Nair *et al.* (2006) explain low bulk crustal V_p/V_s ratios in the Kaapvaal craton through delamination of the basaltic lower crust during collision in an island-arc setting, thereby favouring the uniformitarian view that modern plate tectonics can be used to describe crustal formation in Archaean times. In the Rae domain, however, there is a paucity of evidence to support subduction-related hypotheses. For example, extensive linear orogenic trends in surface geology and potential field maps, which are usually associated with island-arc accretion, are not in evidence (e.g. Eaton & Darbyshire 2010). The absence of greenstone terranes associated with collisional tectonics in the Rae domain (e.g. Hartlaub *et al.* 2004) also makes accretionary crustal formation models difficult to invoke. The felsic, uniform thickness (*c.* 37 km; Fig. 6a) Rae domain crust, with its remarkably sharp Moho and paucity of evidence for intra-crustal reflectivity (Fig. 5b) thus lacks evidence for modern-style plate tectonics. Models favouring vertical tectonic processes, such as crustal delamination or plume activity, were thus considered better suited to the observations by Thompson *et al.* (2010).

The Meso-to-Neoarchaean Hearne domain has a slightly more complex crust (Fig. 5c) with higher V_p/V_s ratios than the Rae. These properties were interpreted by Thompson *et al.* (2010) as a potentially transitional period between non-plate tectonic and plate tectonic processes. Receiver function results from the Quebec–Baffin segment of the THO, however, map out the first-order shape of the Superior plate under-thrusting Meta Incognita, the southern tip of the Churchill collage (Fig. 3; Thompson *et al.* 2010). The elevated V_p/V_s ratios in this region (Fig. 6b) are considered to be representative of the rifted margin of the Superior craton. Markedly thicker crust (*c.* 43 km; Fig. 6a) compared with that observed in the Archaean domains is coincident with widespread medium to high-grade metamorphic geology outcropping at the surface (e.g. St-Onge *et al.* 2006) and can be explained by crustal thickening owing to stacking of accreted terranes during continent–continent collision, analogous to the present-day Tibetan Plateau, followed by erosion (Thompson *et al.* 2010), consistent with the hypothesis of St-Onge *et al.* (2006).

From SKS splitting analysis of seismic anisotropy, Bastow *et al.* (2011*b*) and Snyder *et al.* (2013, with support from receiver functions) showed that fast polarization directions in northern Hudson Bay parallel THO structural trends at the surface (Fig. 9). Relatively large splitting delay times (δt up to 1.45 s) require a relatively thick anisotropic layer (and thus major plate-scale deformation), which Bastow *et al.* (2011*b*) cited as evidence that plate tectonics was in operation by Palaeoproterozoic times at the latest. Corroborating this conclusion, Snyder *et al.* (2013) presented evidence for gently dipping lithospheric layers deep beneath the SE Rae craton, consistent with under-thrusting beneath the Hearne and Meta Incognita Sugluk blocks (Fig. 3). The new tomographic images presented in this study also yield evidence for plate-scale under-thrusting beneath Meta Incognita (Fig. 17a, b, f). In contrast there is little evidence in our new wavespeed maps for such large-scale tectonic processes across the Rae–Hearne domains to the west of Baffin Island (Fig. 17a, b, g).

Taken together, the results from the receiver function, SKS and tomography studies support a model for secular evolution in processes of crustal formation formation, with non-plate tectonic processes during the Palaeoarchaean evolving towards fully developed plate tectonics by the Palaeoproterozoic (Thompson *et al.* 2010).

Based on joint tomographic inversion of ambient-noise and teleseismic Rayleigh-wave dispersion measurements, Pawlak *et al.* (2012) documented systematic variations in anisotropic fabric moving from the upper crust, to the lower crust

Downloaded from http://sp.lyellcollection.org/ at University of Aberdeen on November 26, 2014

and uppermost mantle beneath Hudson Bay. In particular, while anisotropic fabrics in the upper crust and uppermost mantle are consistent with tectonic fabrics created during the THO, lower-crustal fabrics exhibit a more uniform north–south orientation. By analogy with models for crustal evolution in the modern Himalayan orogen, Pawlak *et al.* (2012) interpreted this pattern as evidence for frozen channel flow in the lower crust that formed during the culmination of the orogenic cycle. This model furnishes additional evidence that modern-style plate tectonics was in operation *c.* 1.8 Ga during the THO.

Implications for the formation of the Laurentian keel

The tectosphere or lithospheric mantle beneath cratons commonly extends to depths of 250 km or more into the mantle. These 'keels' have remained stable, resistant to thermal and mechanical erosion during multiple Wilson cycles over billions of years. Archaean processes, such as the extraction of komatiitic magmas (e.g. Griffin *et al.* 2003), are often invoked to explain the intrinsic low density, but the Laurentian keel does not fit easily into the Archaean formation paradigm: it extends below both Archaean and Palaeoproterozoic terranes. Precisely how the keel beneath Hudson Bay formed is thus unclear. Is the present-day keel a relict of initial craton formation in the Archaean (e.g. Sleep 2003), or do later tectonic processes (specifically the THO) also play a role, perhaps resulting in a vertically stratified lithosphere? Stratification of cratonic lithosphere has been inferred previously from both geophysical (Fishwick & Reading 2008; Angus *et al.* 2009; Abt *et al.* 2010; Yuan & Romanowicz 2010) and geochemical/thermobarometric studies (Griffin *et al.* 2003, 2004). The upper lithospheric layer has been interpreted as a highly melt-depleted peridotite chemical boundary layer; the lower, more fertile layer has been described as a thermal boundary layer, formed at a later stage in keel evolution (e.g. Lee *et al.* 2011). *S* to *P* converted phases isolated in receiver function studies, initially interpreted as the LAB (Rychert & Shearer 2009), are strong evidence for the latter hypothesis, and have been cited as evidence for mid-lithospheric discontinuities beneath the Canadian shield (Abt *et al.* 2010; Yuan & Romanowicz 2010).

The new tomographic images presented in this study (Fig. 17) provide compelling evidence that Palaeoproterozoic mantle associated with the THO has been trapped between the Archaean cores of the Superior plate in the south and the Churchill collage (including Meta Incognita and the Sugluk block: Fig. 3) in the north. Depth resolution in such body wave models is never as good as lateral resolution (Fig. 16), but the inferred trapped low-wavespeed material between the Superior craton and the Churchill collage in Figure 17e is certainly a deep-seated lithospheric feature, not the smeared result of crustal structure.

The surface wave study of Darbyshire *et al.* (2013), which solved simultaneously for isotropic phase velocity heterogeneity and azimuthal anisotropy, also suggested a multi-stage assembly of the central Laurentian keel in the Archaean and Palaeoproterozoic. The Darbyshire *et al.* (2013) model (Fig. 12) shows that, in the uppermost mantle, probably associated with the development of the intracratonic basin, seismic wavespeeds immediately beneath Hudson Bay are lower than beneath the surrounding Archaean blocks, and anisotropic fast directions wrap around the Bay. In contrast, in the 70–160 km depth range, the model shows two fast-wavespeed cores beneath the central Superior and Churchill cratons, separated by a near-vertical corridor of lower-wavespeed material. The geometry of this heterogeneous pattern prompted Darbyshire *et al.* (2013) to suggest that it arises from the terminal collision of the Superior and Churchill cratons, trapping more juvenile Proterozoic mantle between them during the THO. In this depth range, no large-scale coherency in anisotropic pattern is evident. However, in the deepest parts of the lithosphere the model reveals significantly more homogeneous velocity structure than the mid-lithosphere. Anisotropy within this layer is coherent, with a pattern strongly reminiscent of the inferred geometry of the THO suture. Given this distinctive deformation pattern, the basal layer is postulated to have accreted to the base of the Archaean cratonic lithosphere during or shortly after the terminal phases of the THO (Darbyshire *et al.* 2013).

Neotectonics, and implications for the development of the Hudson Bay basin

The Hudson Bay basin is the least studied of four major Phanerozoic intracratonic basins (including Williston, Illinois and Michigan) in North America and the mechanism by which it formed remains ambiguous. A number of hypotheses have been proposed over the years, each of which the HuBLE project has tested.

According to one hypothesis, subsidence occurred as a result of convective down-welling within the mantle (e.g. James 1992; Peltier *et al.* 1992). This explanation has also been championed to explain the long-wavelength negative gravity anomaly beneath Hudson Bay (Simons & Hager 1997; Mitrovica 1997; Tamisiea *et al.* 2007). The

Downloaded from http://sp.lyellcollection.org/ at University of Aberdeen on November 26, 2014

receiver function study of Thompson *et al.* (2011) addressed the issue of whether or not a mantle down-welling exists below the Bay by constraining the thermal structure of the mantle at transition zone depths. Elevated mantle temperatures are expected to reduce the depth interval between the olivine-to-wadsleyite (the '410'), and ringwoodite-to-perovskite + magnesiowüstite (the '660') phase transitions in the olivine system; reduced temperatures in the same depth range will increase transition zone thickness (e.g. Bina & Wood, 1987; Ita & Stixrude 1992; Helffrich 2000). The Thompson *et al.* (2011) study showed, however, that beneath the majority of cratonic North America, mantle transition zone seismic discontinuities are unperturbed with respect to the global mean, with the implication that there is little thermal variation at TZ depths beneath the Laurentian keel (Fig. 13). This suggests that any mantle down-welling associated with the long-wavelength negative gravity anomaly, and the Hudson Bay basin itself, must be confined to upper mantle depths. Small-scale convection around the Laurentian keel, if it operates at all, must also be confined to upper mantle depths of $<$410 km (Thompson *et al.* 2011).

Two hypotheses for Hudson Bay basin formation concern the topography generated solely by crustal processes. In the first of these, basin subsidence was triggered by eclogite phase transformation within an orogenic crustal root (Fowler & Nisbet 1985; Eaton & Darbyshire 2010); according to the second, basin subsidence occurred in response to lithospheric extension that resulted in crustal thinning (Hanne *et al.* 2004). These hypotheses make different, testable, predictions about crustal thickness trends. The receiver function study of Thompson *et al.* (2010) was unable to constrain crustal structure beneath the Bay itself, but notably yielded no evidence for an eclogitized lowermost crust beneath its islands and coastal areas: such an assemblage around the Moho would result in gradational, not sharp, *P* to *S* conversions from the Moho, as are observed in Figure 5b & c (compare, for example, to results from the China craton presented by Zheng *et al.* 2008).

The study of ambient noise tomography by Pawlak *et al.* (2011) did, however, place new constraints on crustal structure beneath Hudson Bay. Tomographic maps and cross-sections obtained in the 5–40 s period range (Fig. 7) reveal markedly lower velocities at crustal depths beneath Hudson Bay than in the surrounding Archaean cratons (3.10 ± 0.03 km s^{-1} within Hudson Bay v. 3.18 ± 0.03 km s^{-1} in the Superior craton). The lowest mid-crustal velocities correspond to the region of maximum plate stretching near the centre of the basin, as inferred by Hanne *et al.* (2004). Pawlak *et al.* (2011) present the first compelling direct evidence (the upwarp of mantle material) for crustal thinning beneath the Bay, obviating the need for eclogitization of a remnant lower crustal root as a mechanism for basin formation.

Analysing intra-plate seismicity in the northern part of Hudson Bay (Fig. 8), Steffen *et al.* (2012) noted that waveforms from these small earthquakes are consistent with thrust-fault mechanisms, as inferred from previous studies for the region, as well as model predictions for glacial isostatic adjustment. Present-day crustal stresses are thus influenced by both glacial rebound and pre-existing faults. Hudson Bay itself is an ephemeral feature (*c.* 15 ka), caused by combined incomplete glacial rebound, mantle flow-driven dynamic topography and the thermochemical structure of the Laurentian keel. The seismological results from HuBLE, when synthesized in light of the sedimentary basin study of Hanne *et al.* (2004), and more recent back-stripping studies of the Hudson Bay basin (Pinet *et al.* 2013), suggest strongly that plate stretching is the primary mechanism responsible for the formation of the Hudson Bay basin.

Conclusions

The Hudson Bay lithospheric experiment has placed fundamental new constraints on the crust and upper mantle seismic structure of Laurentia. Highlights of the experiment (so far) include:

- The strong age-dependence on crustal architecture and bulk crustal properties (crustal thickness and V_p/V_s ratio) indicates a secular evolution in processes of crustal formation formation, with non-plate tectonic processes during the Palaeoarchaean evolving towards fully developed plate tectonics by the Palaeoproterozoic.
- Seismic anisotropy, revealed by SKS splitting and surface wave analysis, indicates the preservation of a fossil lithospheric fabric, interpreted as evidence for modern-day-style plate tectonics operating by Palaeoproterozoic times.
- Seismic tomographic images of mantle structure reveal an age dependence of seismic wavespeed: the Archaean cores of Laurentia exhibit faster seismic velocities than Proterozoic material within the heart of Laurentia, trapped since the THO. State-of-the-art anisotropic surface-wave inversions indicate depth-dependent anisotropy. Taken together with the variable wavespeeds across the shield, and evidence for mid-lithospheric discontinuities in *S*–*P* receiver function studies, this implies that cratonic keel formation is not confined to Archaean times.
- Deep beneath the Laurentian lithosphere, a mantle transition zone study shows that the olivine phase transitions from olivine to

Downloaded from http://sp.lyellcollection.org/ at University of Aberdeen on November 26, 2014

wadsleyite (the '410') and from ringwoodite to perovskite + magnesiowüstite (the '660') are at remarkably normal levels across the Laurentian keel's *c.* 3500 km lateral extent. This implies that the keel has no significant thermal effect on the underlying mantle ($\leq$50 K), and any small-scale convection or cold mantle down-welling associated with the large free-air gravity anomaly beneath the Laurentian shield must be confined to the upper mantle above the transition zone (i.e. shallower than 410 km).

- Evidence for crustal thinning beneath the Bay, inferred from ambient noise tomography, indicates that the Hudson Bay basin probably owes its existence to shallow Phanerozoic tectonic processes (plate stretching), not deeper mantle down-wellings.

The UK component of HuBLE was supported by Natural Environment Research Council (NERC) grant NE/F007337/1, with financial and logistical support from the Geological Survey of Canada, Canada–Nunavut Geoscience Office, SEIS-UK (the seismic node of NERC), and First Nations communities of Nunavut. J. Beauchesne and J. Kendall provided invaluable assistance in the field. Discussions with M. St-Onge, T. Skulski, D. Corrigan and M. Sanborne-Barrie were helpful for interpretation of the data. D. Eaton and F. A. Darbyshire acknowledge the Natural Sciences and Engineering Research Council. Four stations on the Belcher Islands and northern Quebec were installed by the University of Western Ontario and funded through a grant to D. Eaton (UWO Academic Development Fund). I. Bastow is funded by the Leverhulme Trust. This is Natural Resources Canada Contribution 20130084 to its Geomapping for Energy and Minerals Program. This work has received funding from the European Research Council under the European Unions Seventh Framework Programme (FP7/2007-2013)/ERC Grant agreement no. 240473 'CoMITAC'.

References

Abt, D., Fischer, K., French, S., Ford, H., Yuan, H. & Romanowicz, B. 2010. North American lithospheric discontinuity structure imaged by Ps and Sp receiver functions. *Journal of Geophysical Research*, **115**, B09301, http://dx.doi.org/10.1029/2009JB006914

Angus, D. A., Kendall, J. M., Wilson, D. C., White, D. J., Sol, S. & Thomson, C. J. 2009. Stratigraphy of the Archean western Superior Province from *P*- and *S*-wave receiver functions: further evidence for tectonic accretion? *Physics of the Earth and Planetary Interiors*, **177**, 206–216, http://dx.doi.org/10.1016/j.pepi.2009.09.002

Artemieva, I. 2006. Global 1 × 1 thermal model TC1 for the continental lithosphere: implications for lithosphere secular evolution. *Tectonophysics*, **416**, 245–277.

Assumpção, M., Heintz, M., Vauchez, A. & Silva, M. 2006. Upper mantle anisotropy in SE and central Brazil from SKS splitting: evidence of asthenospheric flow around a cratonic keel. *Earth and Planetary Science Letters*, **250**, 224–240, http://dx.doi.org/10.1016/j.epsl.2006.07.038

Basham, P., Forsyth, D. & Wetmiller, R. 1977. The seismicity of northern Canada. *Canadian Journal of Earth Sciences*, **14**, 1646–1667.

Bastow, I. D., Stuart, G. W., Kendall, J.-M. & Ebinger, C. 2005. Upper-mantle seismic structure in a region of incipient continental breakup: northern Ethiopian rift. *Geophysical Journal International*, **162**, 479–493, http://dx.doi.org/10.1111/j.1365-246X.2005.02666.x

Bastow, I. D., Owens, T. J., Helffrich, G. & Knapp, J. 2007. Spatial and temporal constraints on sources of seismic anisotropy: evidence from the Scottish highlands. *Geophysical Research Letters*, **34**, L05305, http://dx.doi.org/10.1029/2006GL028911

Bastow, I. D., Nyblade, A. A., Stuart, G. W., Rooney, T. O. & Benoit, M. H. 2008. Upper mantle seismic structure beneath the Ethiopian hotspot: rifting at the edge of the African Low Velocity Anomaly. *Geochemistry, Geophysics, Geosystems*, **9**, Q12022, http://dx.doi.org/10.1029/2008GC002107

Bastow, I. D., Kendall, J.-M. *et al.* 2011*a*. The Hudson Bay Lithospheric Experiment. *Astronomy and Geophysics*, **52**, 21–24, http://dx.doi.org/10.1111/j.1468-4004.2011.52621.x

Bastow, I. D., Thompson, D. *et al.* 2011*b*. Precambrian plate tectonics: seismic evidence from northern Hudson Bay, Canada. *Geology*, **39**, 91–94, http://dx.doi.org/10.1130/G31396.1

Bedle, H. & van der Lee, S. 2009. *S* velocity variations beneath North America. *Journal of Geophysical Research*, **114**, B07308, http://dx.doi.org/10.1029/2008JB005949

Berman, R., Sanborn-Barrie, M., Stern, R. & Carson, C. 2005. Tectonometamorphism at ca. 2.35 and 1.85 Ga in the Rae domain, western Churchill Province, Nunavut, Canada: insights from structural, metamorphic and in situ geochronological analysis of the southwestern Committee Bay Belt. *The Canadian Mineralogist*, **43**, 409–442, http://dx.doi.org/10.2113/gscanmin.43.1.409

Berman, R., Davis, W. & Pehrsson, S. 2007. Collisional Snowbird tectonic zone resurrected: growth of Laurentia during the 1.9 Ga accretionary phase of the Hudsonian orogeny. *Geology*, **35**, 911–914, http://dx.doi.org/10.1130/G23771A.1

Berman, R., Sanborn-Barrie, M., Rayner, N., Carson, C., Sandeman, H. & Skulski, T. 2010*a*. Petrological and in situ SHRIMP geochronological constraints on the tectonometamorphic evolution of the Committee Bay belt, Rae Province, Nunavut. *Precambrian Research*, **181**, 1–20, http://dx.doi.org/10.1016/j.precamres.2010.05.009

Berman, R., Sandeman, H. & Camacho, A. 2010*b*. Diachronous Palaeoproterozoic deformation and metamorphism in the Committee Bay belt, Rae Province, Nunavut: insights from ^{40}Ar–^{39}Ar cooling ages and thermal modeling. *Journal of Metamorphic Geology*, **328**, 439–457, http://dx.doi.org/10.1111/j.1525-1314.2010.00873.x

Berman, R. G., Pehrsson, S., Davis, W. J., Ryan, J. J., Qui, H. & Ashton, K. E. 2013. The Arrowsmith orogeny: geochronological and thermobarometric

Downloaded from http://sp.lyellcollection.org/ at University of Aberdeen on November 26, 2014

constraints on its extent and tectonic setting in the Rae craton, with implications for pre-Nuna supercontinent reconstruction. *Precambrian Research*, **232**, 44–69, http://dx.doi.org/10.1016/j.precamres.2012.10.015

Bethune, K., Hinchey, A., Davis, W., Ryan, J. & Nadeau, L. 2011. Neoarchean high-potassium granites of the Boothia mainland area, Rae domain, Churchill Province: U–Pb zircon and Sm–Nd whole rock isotopic constraints. [This article is one of a series of papers published in this Special Issue on the theme of Geochronology in honour of Tom Krogh.] *Canadian Journal of Earth Sciences*, **48**, 247–279.

Bina, C. & Wood, B. 1987. Olivine–spinel transitions: experimental and thermodynamic constraints and implications for the nature of the 400 km seismic discontinuity. *Journal of Geophysical Research*, **92**, 4853–4866.

Blackman, D. & Kendall, J.-M. 1997. Sensitivity of teleseismic body waves to mineral texture and melt in the mantle beneath a mid-ocean ridge. *Philosophical Transactions of the Royal Society of London*, **355**, 217–231.

Bokelmann, G. & Silver, P. 2002. Shear stress at the base of shield lithosphere. *Geophysical Research Letters*, **29**, 6-1–6-4, http://dx.doi.org/10.1029/2002GL015925

Bostock, M. 1996. *PS* conversions from the upper mantle transition zone beneath the Canadian landmass. *Journal of Geophysical Research*, **101**, 8393–8402, http://dx.doi.org/10.1029/95JB03741

Brune, J. & Dorman, J. 1963. Seismic waves and earth structure in the Canadian Shield. *Bulletin of the Seismological Society of America*, **53**, 167.

Bruneton, M., Pedersen, H. A. *et al.* 2004. Complex lithospheric structure under the central Baltic Shield from surface wave tomography. *Journal of Geophysical Research*, **109**, B10303, http://dx.doi.org/10.1029/2003JB002947

Chevrot, S., Vinnik, L. & Montagner, J. 1999. Global-scale analysis of the mantle PDS phases. *Journal of Geophysical Research*, **104**, 20 203–20 219, http://dx.doi.org/10.1029/1999JB900087

Christensen, N. 1996. Poisson's ratio and crustal seismology. *Journal of Geophysical Research*, **101**, 3139–3156, http://dx.doi.org/10.1029/95JB03446

Constable, S., Parker, R. & Constable, C. 1987. Occam's inversion: a practical algorithm for generating smooth models from electromagnetic sounding data. *Geophysics*, **52**, 289–300, http://dx.doi.org/10.1190/1.1442303

Corrigan, D., Pehrsson, S., Wodicka, N. & de Kemp, E. 2009. The Palaeoproterozoic Trans-Hudson Orogen: a prototype of modern accretionary processes. *In*: Murphy, J. B., Keppie, J. D. & Hynes, A. J. (eds) *Ancient Orogens and Modern Analogues*. Geological Society, London, Special Publications, **327**, 457–479, http://dx.doi.org/10.1144/SP327.19

Darbyshire, F. 2005. Upper mantle structure of Arctic Canada from Rayleigh wave dispersion. *Tectonophysics*, **405**, 1–23, http://dx.doi.org/10.1016/j.tecto.2005.02.013

Darbyshire, F. & Eaton, D. 2010. The lithospheric root beneath Hudson Bay, Canada from Rayleigh wave dispersion: no clear seismological distinction between Archean and Proterozoic mantle. *Lithos*, **120**, 144–159, http://dx.doi.org/10.1016/j.lithos.2010.04.010

Darbyshire, F., Eaton, D., Frederiksen, A. & Ertolahti, L. 2007. New insights into the lithosphere beneath the Superior Province from Rayleigh wave dispersion and receiver function analysis. *Geophysical Journal International*, **169**, 173–1067, http://dx.doi.org/10.1111/j.1365-246X.2006.03259.x

Darbyshire, F. A., Eaton, D. W. & Bastow, I. D. 2013. Seismic imaging of the lithosphere beneath Hudson Bay: episodic growth of the Laurentian mantle keel. *Earth and Planetary Science Letters*, **373**, 179–193, http://dx.doi.org/10.1016/j.epsl.2013.05.002

Davis, W., Hanmer, S. & Sandeman, H. 2004. Temporal evolution of the Neoarchean Central Hearne supracrustal belt: rapid generation of juvenile crust in a supra subduction zone setting. *Precambrian Research*, **134**, 85–112, http://dx.doi.org/10.1016/j.precamres.2004.02.002

Davis, W., Hanmer, S., Tella, S., Sandeman, H. & Ryan, J. 2006. U–Pb geochronology of the MacQuoid supracrustal belt and Cross Bay plutonic complex: key components of the northwestern Hearne subdomain, western Churchill Province, Nunavut, Canada. *Precambrian Research*, **145**, 53–80, http://dx.doi.org/10.1016/j.precamres.2005.11.016

Debayle, E., Kennett, B. & Priestley, K. 2005. Global azimuthal seismic anisotropy and the unique plate-motion deformation of Australia. *Nature*, **433**, 509–512, http://dx.doi.org/10.1038/nature03247

Di Leo, J., Wookey, J. *et al.* 2012. Deformation and mantle flow beneath the Sangihe subduction zone from seismic anisotropy. *Physics of the Earth and Planetary Interiors*, **194**, 38–54, http://dx.doi.org/10.1016/j.pepi.2012.01.008

Durrheim, R. J. & Mooney, W. D. 1994. Evolution of the Precambrian lithosphere: seismological and geochemical constraints. *Journal of Geophysical Research*, **99**, 15 359–15 374.

Eaton, D. & Darbyshire, F. 2010. Lithospheric architecture and tectonic evolution of the Hudson Bay region. *Tectonophysics*, **480**, 1–22, http://dx.doi.org/10.1016/j.tecto.2009.09.006

Eaton, D. & Frederiksen, A. 2007. Seismic evidence for convection-driven motion of the North American plate. *Nature*, **446**, 428–431, http://dx.doi.org/10.1038/nature05675

Eaton, D., Adams, J. *et al.* 2005. Investigating Canada's lithosphere and earthquake hazards with portable arrays. *EOS Transactions AGU*, **86**, 169–173, http://dx.doi.org/10.1029/2005EO170001

Eaton, D., Darbyshire, F., Evans, R., Grütter, H., Jones, A. & Yuan, X. 2009. The elusive lithosphere–asthenosphere boundary (LAB) beneath cratons. *Lithos*, **109**, 1–22, http://dx.doi.org/10.1016/j.lithos.2008.05.009

Fishwick, S. & Reading, A. M. 2008. Anomalous lithosphere beneath the Proterozoic of western and central Australia: a record of continental collision and intraplate deformation? *Precambrian Research*, **166**, 111–121, http://dx.doi.org/10.1016/j.precamres.2007.04.026

Fishwick, S., Kennett, B. & Reading, A. 2005. Contrasts in lithospheric structure within the Australian

Downloaded from http://sp.lyellcollection.org/ at University of Aberdeen on November 26, 2014

craton – insights from surface wave tomography. *Earth and Planetary Science Letters*, **231**, 163–176, http://dx.doi.org/10.1016/j.epsl.2005.01.009

Flanagan, M. & Shearer, P. 1998. Global mapping of topography on transition zone velocity discontinuities by stacking SS precursors. *Journal of Geophysical Research*, **103**, 2673–2692, http://dx.doi.org/10.1029/97JB03212

Fouch, M., Fischer, A., Parmentier, E., Wysession, M. & Clarke, T. 2000. Shear wave splitting, continental keels and patterns of mantle flow. *Journal of Geophysical Research*, **105**, 6255–6276, http://dx.doi.org/10.1029/1999JB900372

Fowler, C. & Nisbet, E. 1985. The subsidence of the Williston Basin. *Canadian Journal of Earth Sciences*, **22**, 408–415.

Frederiksen, A., Miong, S., Darbyshire, F., Eaton, D., Rondenay, S. & Sol, S. 2007. Lithospheric variations across the Superior Province, Ontario, Canada: evidence from tomography and shear wave splitting. *Journal of Geophysical Research*, **112**, B07318, http://dx.doi.org/10.1029/2006JB004861

Goes, S. & van der Lee, S. 2002. Thermal structure of the North American uppermost mantle inferred from seismic tomography. *Journal of Geophysical Research*, **107**, http://dx.doi.org/10.1029/2000JB000049

Goes, S., Govers, R. & Vacher, P. 2000. Shallow mantle temperatures under Europe from *P* and *S* wave tomography. *Journal of Geophysical Research*, **105**, 11 153–11 169, http://dx.doi.org/10.1029/1999JB900300

Gossler, J. & Kind, R. 1996. Seismic evidence for very deep roots of continents. *Earth and Planetary Science Letters*, **138**, 1–13, http://dx.doi.org/10.1016/0012-821X(95)00215-X

Griffin, W., Oreilly, S. *et al.* 2003. The origin and evolution of Archean lithospheric mantle. *Precambrian Research*, **127**, 19–41, http://dx.doi.org/10.1016/S0301-9268(03)00180-3

Griffin, W., O'Reilly, S. *et al.* 2004. Lithosphere mapping beneath the North American plate. *Lithos*, **77**, 873–922.

Gripp, A. & Gordon, R. 2002. Young tracks of hotspots and current plate velocities. *Geophysical Journal International*, **150**, 321–361, http://dx.doi.org/10.1046/j.1365-246X.2002.01627.x

Gu, Y. & Dziewonski, A. 2002. Global variability of transition zone thickness. *Journal of Geophysical Research*, **107**, http://dx.doi.org/10.1029/2001JB000489

Gu, Y., Dziewonski, A. & Agee, C. 1998. Global de-correlation of the topography of transition zone discontinuities. *Earth and Planetary Science Letters*, **157**, 57–67, http://dx.doi.org/10.1016/S0012-821X(98)00027-2

Hales, A. 1969. A seismic discontinuity in the lithosphere. *Earth and Planetary Science Letters*, **7**, 44–46.

Hanne, D., White, N., Butler, A. & Jones, S. 2004. Phanerozoic vertical motions of Hudson Bay. *Canadian Journal of Earth Sciences*, **41**, 1181–1200, http://dx.doi.org/10.1139/E04-047

Hartlaub, R. P., Heaman, L. M., Ashton, K. E. & Chacko, T. 2004. The Archean Murmac Bay Group: vidence for a giant Archean rift in the Rae Province, Canada. *Precambrian Research*, **131**, 345–372, http://dx.doi.org/10.1016/j.precamres.2004.01.001

Helffrich, G. 2000. Topography of the transition zone seismic discontinuities. *Reviews of Geophysics*, **38**, 141–158, http://dx.doi.org/10.1029/1999RG000060

Helffrich, G. 2006. Extended-time multitaper Frequency domain cross-correlation receiver-function estimation. *Bulletin of the Seismological Society of America*, **96**, 344–347, http://dx.doi.org/10.1785/0120050098

Hobson, G. 1967. Hudson Bay crustal seismic experiment: time and distance data. *Canadian Journal of Earth Sciences*, **4**, 879–899.

Hoffman, P. 1988. United Plates of America, the birth of a craton – Early Proterozoic assembly and growth of Laurentia. *Annual Reviews of Earth and Planetary Sciences*, **16**, 543–603, http://dx.doi.org/10.1146/annurev.ea.16.050188.002551

Hoffman, P. 1990. Geological constraints on the origin of the mantle root beneath the Canadian Shield. *Philosophical Transactions of the Royal Society of London A*, **331**, 523–532.

Hopkins, M., Harrison, T. & Manning, C. 2008. Low heat flow inferred from 4 Gyr zircons suggests Hadean plate boundary interactions. *Nature*, **456**, 493–496, http://dx.doi.org/10.1038/nature07465

Ita, J. & Stixrude, L. 1992. Petrology, elasticity and composition of the mantle transition zone. *Journal of Geophysical Research*, **97**, 849–6.

Jackson, G. 1966. Geology and mineral possibilities of the Mary River region, northern Baffin Island. *Canadian Mineralogist*, **87**, 57–61.

James, T. 1992. The Hudson Bay free-air gravity anomaly and glacial rebound. *Geophysical Research Letters*, **19**, 861–864, http://dx.doi.org/10.1029/92GL00687

Jordan, T. 1978. Composition and development of the continental tectosphere. *Nature*, **274**(5671), 544–548.

Jordan, T. 1988. Structure and formation of the continental tectosphere. *Journal of Petrology*, Special Lithosphere Issue, 11–37.

Karato, S. 1993. Importance of anelasticity in the interpretation of seismic tomography. *Geophysical Research Letters*, **20**, 1623–1626, http://dx.doi.org/10.1029/93GL01767

Kay, I., Sol, S. S. *et al.* 1999. Shear wave splitting observations in the Archean craton of Western Superior. *Geophysical Research Letters*, **26**, 2669–2672.

Kendall, J. M., Sol, S., Thomson, C. J., White, D. J., Asudeh, I., Snell, C. S. & Sutherland, F. H. 2002. Seismic heterogeneity and anisotropy in the Western Superior Province, Canada: insights into the evolution of an Archaean craton. *In*: Fowler, C. M. R., Ebinger, C. J. & Hawkesworth, C. J. (eds) *The Early Earth: Physical, Chemical and Biological Development*. Geological Society, London, Special Publications, **199**, 27–44.

Kennett, B. & Engdahl, E. 1991. Traveltimes from global earthquake location and phase identification. *Geophysical Journal International*, **105**, 429–465.

Kumar, P., Kind, R., Yuan, X. & Mechie, J. 2012. USArray receiver function images of the lithosphere–asthenosphere boundary. *Seismological Research Letters*, **83**, 486–491.

Downloaded from http://sp.lyellcollection.org/ at University of Aberdeen on November 26, 2014

Langston, C. 1979. Structure under Mount Rainer, Washington, inferred from teleseismic body waves. *Journal of Geophysical Research*, **84**, 4749–4762.

Lawrence, J. & Shearer, P. 2006. A global study of transition zone thickness using receiver functions. *Journal of Geophysical Research*, **111**, B06307, http://dx.doi.org/10.1029/2005JB003973

Lebedev, S. & van der Hilst, R. 2008. Global upper-mantle tomography with the automated multimode inversion of surface and *S*-wave forms. *Geophysical Journal International*, **173**, 505–518, http://dx.doi.org/10.1111/j.1365-246X.2008.03721.x

Lebedev, S., Boonen, J. & Trampert, J. 2009. Seismic structure of Precambrian lithosphere: new constraints from broad-band surface-wave dispersion. *Lithos*, **109**, 96–111, http://dx.doi.org/10.1016/j.lithos.2008.06.010

Lee, C., Luffi, P. & Chin, E. 2011. Building and destroying continental mantle. *Annual Reviews of Earth and Planetary Sciences*, **39**, 59–90, http://dx.doi.org/10.1146/annurev-earth-040610-133505

Lévy, F., Jaupart, C., Mareschal, J., Bienfait, G. & Limare, A. 2010. Low heat flux and large variations of lithospheric thickness in the Canadian Shield. *Journal of Geophysical Research*, **115**, B06404, http://dx.doi.org/10.1029/2009JB006470

Li, A. & Burke, K. 2006. Upper mantle structure of southern Africa from Rayleigh wave tomography. *Journal of Geophysical Research*, **111**, http://dx.doi.org/10.1029/2006JB004321

Li, A., Fischer, K., Wysession, M. & Clarke, T. 1998. Mantle discontinuities and temperature under the North American continental keel. *Nature*, **395**, 160–163.

Li, C., van der Hilst, R., Engdahl, R. & Burdick, S. 2008. A new global model for *P* wave speed variations in Earth's mantle. *Geochemistry, Geophysics, Geosystems*, **9**, Q05018, http://dx.doi.org/10.1029/2007GC001806

Marone, F. & Romanowicz, B. 2007. The depth distribution of azimuthal anisotropy in the continental upper mantle. *Nature*, **447**, 7141, http://dx.doi.org/10.1038/nature05742

Megnin, C. & Romanowicz, B. 2000. The three-dimensional shear velocity structure of the mantle from the inversion of body, surface and higher-mode waveforms. *Geophysical Journal International*, **143**, 709–728, http://dx.doi.org/10.1046/j.1365-246X.2000.00298.x

Miller, M. & Eaton, D. 2010. Formation of cratonic mantle keels by arc accretion: evidence from *S* receiver functions. *Geophysical Research Letters*, **37**, L18305, http://dx.doi.org/10.1029/2010GL044366

Mitrovica, J. 1997. Geophysics: going halves over Hudson Bay. *Nature*, **390**, 444–447, http://dx.doi.org/10.1038/37231

Nair, S. K., Gao, S. S., Liu, K. H. & Silver, P. G. 2006. Southern African crustal evolution and composition: constraints from receiver function studies. *Journal of Geophysical Research*, **111**, B02304, http://dx.doi.org/10.1029/2005JB003802

Nettles, M. & Dziewonski, A. 2008. Radially anisotropic shear velocity structure of the upper mantle globally and beneath North America. *Journal of Geophysical Research*, **113**, B02303, http://dx.doi.org/10.1029/2006JB004819

Pawlak, A., Eaton, D. W., Bastow, I. D., Kendall, J.-M., Helffrich, G., Wookey, J. & Snyder, D. B. 2011. Crustal structure beneath Hudson Bay from ambient noise tomography: implications for basin formation. *Geophysical Journal International*, **184**, 65–82, http://dx.doi.org/10.1111/j.1365-246X.2010.04828.x

Pawlak, A., Eaton, D. W., Lebedev, S., Darbyshire, F. A. & Bastow, I. D. 2012. Crustal anisotropy beneath Hudson Bay from ambient-noise tomography: evidence for post-orogenic lower-crustal flow? *Geophysical Journal International*, **117**, B08301, http://dx.doi.org/10.1029/2011JB009066

Peltier, W., Forte, A., Mitrovica, J. & Dziewonski, A. 1992. Earth's gravitational field: seismic tomography resolves the enigma of the Laurentian Anomaly. *Geophysical Research Letters*, **19**, 1555–1558.

Pinet, N., Lavoi, D., Dietrich, J., Hu, K. & Keating, P. 2013. Architecture and subsidence history of the intracratonic Hudson Bay Basin, northern Canada. *Earth-Science Reviews*, http://dx.doi.org/10.1016/j.earscirev.2013.05.010

Poupinet, G. 1979. On the relation between *P*-wave travel time residuals and the age of the continental plates. *Earth and Planetary Science Letters*, **43**, 149–161.

Ritsema, J., Nyblade, A., Owens, T., Langston, C. & VanDecar, J. 1998. Upper mantle seismic velocity structure beneath Tanzania, East Africa: implications for the stability of cratonic lithosphere. *Journal of Geophysical Research*, **103**, 201–21, 213.

Ritsema, J., Deuss, A., van Heijst, H. & Woodhouse, J. 2011. S40RTS: a degree-40 shear-velocity model for the mantle from new Rayleigh wave dispersion, teleseismic traveltime and normal-mode splitting function measurements. *Geophysical Journal International*, **184**, 1223–1236, http://dx.doi.org/10.1111/j.1365-246X.2010.04884.x

Roksandic, M., Beaumont, C. & Tabkyard, A. 1987. The tectonics and evolution of the Hudson Bay region. *Canadian Society of Petroleum Geologists Memoir*, **12**, 507–518.

Rudnick, R. L. 1995. Making continental crust. *Nature*, **378**, 571–578.

Ruffman, A. & Keen, M. 1967. A time-term analysis of the first arrival data from the seismic experiment in Hudson Bay, 1965. *Canadian Journal of Earth Sciences*, **4**, 901–928.

Rychert, C. & Shearer, P. 2009. A global view of the lithosphere–asthenosphere boundary. *Science*, **3245926**, 495–498.

Schultz, M., Chacko, T., Heaman, L., Sandeman, H., Simonetti, A. & Creaser, R. 2007. Queen Maud block: a newly recognized Paleoproterozoic (2.4–2.5 Ga) terrane in northwest Laurentia. *Geology*, **35**, 707–710.

Scott, D. 1997. Geology, U–Pb and Pb–Pb geochronology of the Lake Harbour area, southern Baffin Island: implications for the Paleoproterozoic tectonic evolution of northeastern Laurentia. *Canadian Journal of Earth Sciences*, **34**, 140–155.

Shapiro, N. & Ritzwoller, M. 2002. Monte-Carlo inversion for a global shear-velocity model of the crust and

Downloaded from http://sp.lyellcollection.org/ at University of Aberdeen on November 26, 2014

upper mantle. *Geophysical Journal International*, **151**, 88–105.

Shapiro, N., Campillo, M., Stehly, L. & Ritzwoller, M. 2005. High-resolution surface-wave tomography from ambient seismic noise. *Science*, **307**, 1615–1618.

Silver, P. & Chan, G. 1991. Shear wave splitting and subcontinental mantle deformation. *Journal of Geophysical Research*, **96**, 429–16,454.

Simons, M. & Hager, B. 1997. Localization of the gravity field and the signature of glacial rebound. *Nature*, **390**, 6659.

Simons, F., Zielhuis, A. & van der Hilst, R. 1999. The deep structure of the Australian continent from surface wave tomography. *Lithos*, **48**, 17–43.

Sleep, N. 2003. Survival of Archean cratonal lithosphere. *Journal of Geophysical Research*, **108**, 2302, http://dx.doi.org/10.1029/2001JB000169

Snyder, D., Berman, R., Kendall, J.-M. & Sanborn-Barrie, M. 2013. Seismic anisotropy and mantle structure of the Rae craton, central Canada, from joint interpretation of SKS splitting and receiver functions. *Precambrian Research*, **232**, 189–208, http://dx.doi.org/10.1016/j.precamres.2012.03.003

Sol, S., Thompson, C., Kendall, J.-M., White, D., VanDecar, J. & Asude, I. 2002. Seismic tomographic images of the cratonic upper mantle beneath the Western Superior Province of the Canadian Shield – a remnant Archaean slab. *Physics of the Earth and Planetary Interiors*, **134**, 53–69.

St-Onge, M., Searle, M. & Wodicka, N. 2006. Trans-Hudson Orogen of North America and Himalaya–Karakoram–Tibetan Orogen of Asia: structural and thermal characteristics of the lower and upper plates. *Tectonics*, **25**, http://dx.doi.org/10.1029/2005TC001907

St-Onge, M., Van Gool, J., Garde, A. & Scott, D. 2009. Correlation of Archaean and Palaeoproterozoic units between northeastern Canada and western Greenland: constraining the pre-collisional upper plate accretionary history of the Trans-Hudson orogeny. *In*: Cawood, P. A. & Kröner, A. (eds) *Earth Accretionary Systems in Space and Time*. Geological Society, London, Special Publications, **318**, 193–235, http://dx.doi.org/10.1144/SP318.7

Steffen, R., Eaton, D. & Wu, P. 2012. Moment tensors, state of stress and their relation to postglacial rebound in northeastern Canada. *Geophysical Journal International*, **189**, 1741–1752, http://dx.doi.org/10.1111/j.1365-246X.2012.05452.x

Stern, R. 2005. Evidence from ophiolites, blueschists and ultrahigh-pressure metamorphic terranes that the modern episode of subduction tectonics began in Neoproterozoic time. *Geology*, **33**, 557–560, http://dx.doi.org/10.1130/G21365.1

Tamisiea, M., Mitrovica, J. & Davis, J. 2007. GRACE gravity data constrain ancient ice geometries and continental dynamics over Laurentia. *Science*, **316**, 5826, http://dx.doi.org/10.1126/science.1137157

Thompson, D., Bastow, I., Helffrich, G., Kendall, J.-M., Wookey, J., Snyder, D. & Eaton, D. 2010. Precambrian crustal evolution: seismic constraints from the Canadian Shield. *Earth and Planetary Science Letters*, **297**, 655–666, http://dx.doi.org/10.1016/j.epsl.2010.07.021

Thompson, D., Helffrich, G., Bastow, I., Wookey, J., Kendall, J.-M., Eaton, D. & Snyder, D. 2011. Implications of a simple mantle transition zone beneath cratonic North America. *Earth and Planetary Science Letters*, **312**, 28–36, http://dx.doi.org/10.1016/j.epsl.2011.09.037

Tilmann, F., Benz, H., Priestley, K. & Okubo, P. 2001. *P*-wave velocity structure of the uppermost mantle beneath Hawaii from traveltime tomography. *Geophysical Journal International*, **146**, 594–606.

VanDecar, J. & Crosson, R. 1990. Determination of teleseismic relative phase arrival times using multichannel cross-correlation and least squares. *Bulletin of the Seismological Society of America*, **80**, 150–169.

VanDecar, J., James, D. & Assumpção, M. 1995. Seismic evidence for a fossil mantle plume beneath South America and implications for plate driving forces. *Nature*, **378**, 25–31.

Villemaire, M., Darbyshire, F. & Bastow, I. 2012. *P*-wave tomography of Eastern North America: evidence for mantle evolution from Archean to Phanerozoic and modification during subsequent hotspot tectonism. *Journal of Geophysical Research*, **112**, B12302, http://dx.doi.org/10.1029/2012JB009639

Whalen, J., Wodicka, N., Taylor, B. & Jackson, G. 2010. Cumberland batholith, Trans-Hudson Orogen, Canada: petrogenesis and implications for Paleoproterozoic crustal and orogenic processes. *Lithos*, **117**, 99–118.

Whalen, J., Sanborn-Barrie, M. & Chakungal, J. 2011. Geochemical and Nd isotopic constraints from plutonic rocks on the magmatic and crustal evolution of Southampton Island, Nunavut. *Geological Survey of Canada Current Research (online)*, **2011–2**, 2011, http://dx.doi.org/10.4095/286319

Wodicka, N., Corrigan, D., Nadeau, L. & Erdmann, S. 2011*a*. New U–Pb geochronological results from Melville Peninsula: unravelling the Archean and Early Paleoproterozoic magmatic history of the north-central Rae craton. Abstract 36, Geological Association of Canada–Mineralogical Association of Canada.

Wodicka, N., Corrigan, D., Nadeau, L. & Erdmann, S. 2011*b*. Meta Incognita microcontinent revisited: insights from U–Pb geochronology and Nd isotopes. Abstract 35, Geological Association of Canada–Mineralogical Association of Canada.

Yuan, H. & Romanowicz, B. 2010. Lithospheric layering in the North American craton. *Nature*, **466**, http://dx.doi.org/10.1038/nature09332

Yuan, H., Romanowicz, B., Fischer, K. & Abt, D. 2011. 3-D shear wave radially and azimuthally anisotropic velocity model of the North American upper mantle. *Geophysical Journal International*, **184**, 1237–1260, http://dx.doi.org/10.1111/j.1365-246X.2010.04901.x.

Zheng, T., Zhao, L., Xu, W. & Zhu, R. 2008. Insight into modification of North China Craton from seismological study in the Shandong Province. *Geophysical Research Letters*, **35**, L22305.

Zhu, L. & Kanamori, H. 2000. Moho depth variation in southern California from teleseismic receiver functions. *Journal of Geophysical Research*, **105**, 2969–2980, http://dx.doi.org/10.1029/1999JB900322